XMM Optical Monitor

MULLARD SPACE SCIENCE LABORATORY

UNIVERSITY COLLEGE LONDON

Authors: H. Kawakami, Alice Breeveld and John Fordham*

***** **Dept. Physics and Astronomy, UCL**

Characteristics of the FM intensifiers

Document Number: XMM-OM/MSSL/TC/0054.01 1-July-99

Distribution:

XMM-OM Project Office	A Dibbens	Orig.
University College London	J Fordham	
Mullard Space Science Laboratory	K Mason	
	A Smith	
	P Guttrige	
	J Lapington	
	A Breeveld	
	H Kawakami	

ESTEC R Much

DEP

<< Characteristics of the FM intensifiers >>

XMM-OM/MSSL/TC/0054.01

15 July 1999

Alice's English-version

Hajime Kawakami, Alice Breeveld and John Fordham*

Mullard Space Science Laboratory, University College London

* Dept. of physics and astronomy, University College London

1. Introduction

DEP produced a XMM-OM demonstration intensifier with chevron structure in 1997. Its performance was thoroughly tested at MSSL (XMM-OM/MSSL/TC/0044) and was proven to be deliverable. FM-intensifiers were ordered from DEP in early 1998 with some design changes from the demonstration model to meet mechanical and performance requirements for XMM-OM. A schematic diagram of the FM-intensifier is shown in Fig 1_1. Performance specifications are summarized in table1_1. The main changes of design were

1) photocathode gap = 150um

2) 8um pore diameter on 10um spacing for MCP1

3) P-46 phosphor screen

4) tapered fibre for output interface

By 19 June 1998, DEP (with considerable effort) produced 6 intensifiers for XMM-OM FM, from 3 batches. After completion of each batch, MSSL and DEP held a review meeting and successfully improved the performance, batch by batch. Five intensifiers out of the 6 showed high performance and were flyable. One intensifier, which showed large anode current during manufacturing, was delivered to MSSL as a set-up device.

Unfortunately, it was damaged by arcing between the MCP-out and anode tags during the initial operation test. The last intensifier was produced in Dec 1998 for a ruggedness test, as XMM-OM was delivered to

ESA in the beginning of July. This intensifier employs the same structure as the other FM-intensifiers but does not use space qualified clean material. The production history of the FM intensifiers is summarized in table 1_2.

DEP_#1 and DEP_#4 intensifiers were selected for the primary channel and secondary channel of XMM-OM flight detector, respectively. Not all characteristics, however, were tested for these two FM

intensifiers due

to the tight FM delivery schedule. These characteristics were estimated from the measurements of other intensifiers. Examples are the resolution at UV wavelengths and the Q.E.s.

This document was written for with the intention of helping the XMM-OM science calibration procedure. Archived image data used for this document have been listed in the end of each section, so that a calibration scientist can find the original files easily. The archived data are available in a CD-ROM for calibration scientists.

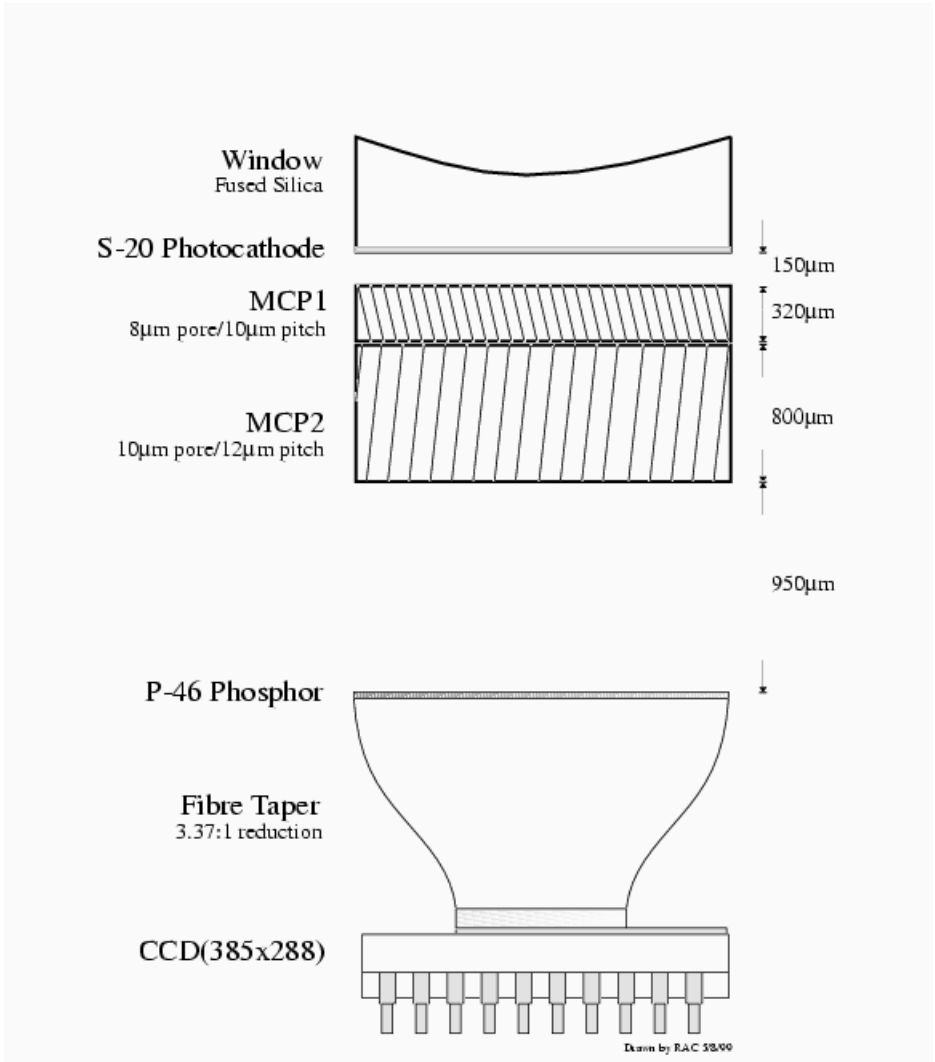

Fig. 1_1 Schematic Structure of Detector Head

Table 1_1.

Requirements for XMM-OM flight intensifier (DEP tube)

Parameter	
Photo-cathode Type	S20
Input Window Material	Hereaus Suprasil. Selected for minimum fluorescence. Concave window, radius of curvature -57.57mm, centre thickness 4mm
Proximity Focusing Gap	150um +/- 50um
First MCP Characteristics	8um pores on 10um centres >= 8 degree bias 40:1 aspect ratio, Manufactured by Galileo
Second MCP Characteristics	10um pores on 12um centres ≥ 8 degrees bias, 80:1 aspect ratio, Manufactured by Galileo
Gap between MCP1 and MCP2	0um
MCP Configuration	Chevron in a Single Plane +/- 5 degrees
MCPs Orientation of bias	Reference mark on MCP2 to be aligned to CCD X-axis (see Appendix) within +/- 2 angle degrees. MCP1 should be rotated slightly so that moire fringe pattern is not noticeable

Phosphor Type	P46
Output Window	Fiber-Optic Taper (MSSL supplied)
Operating Voltage	see Table Sp-1
Photo-cathode RQE @ 20 Celsius	> 20% @300nm, >6% @550nm
Photo-cathode Emission Defects (Defect if >=0.1 counts/sec)	None at Vmax
Photo-cathode Non-Uniformity over 18x18mm area aligned with +/-X CCD axis	<10% rms. of mean over any 50nm interval from 220nm to 550nm
MCP Switched ON Channels (Def. -switched on if dark current >0.05 counts/sec at nominal operating voltages)	None within 18mm x 18mm central area oriented along the +/- X CCD axis
Dark Defects measured at Phosphor (Def. -local area <70%	< 3 between 20um & 80um None larger than 80um

gain)	
MCPs Gain non-uniformity over 18mm x 18mm area, aligned with +/- X CCD axis (see Note 1)	<10% rms. of mean
Dark Counts @20 Celsius	<50 counts/cm**2/sec excluding switched-on channels
Photon Gain (see Note 2)	> 5 x 10**6 photons/photoelectron at peak of the pulse height distribution, tube operated at nominal voltages
Pulse Height Distribution	1. < 130% dG/G FWHM valley height < 30% of peak test area 2mm x 2mm 2. spatial variation of the peak over the whole area of the detector <15% peak to peak (see Note 3) N.B. tube operated at nominal voltages
Maximum Survival Voltage (Note 4)	Photo-cathode to MCP1 : 400V Across MCP1+MCP2 :2800V Across anode gap :6000V
Average Event Width	60um +/- 20um FWHM

Signal Induced	≤ 0.3 per primary event for events of energy
Background	between 5% and 15% of the primary event
	≤ 0.03 per primary event for events with
	energy > 15% of the primary event

Note 1) The 18 x 18 mm area is illuminated with a brightness of >100,000 counts/sec. Integrate for longer than 600 sec (or equivalent) to achieve sufficient S/N

Note 2) Precise Photon Gain is given by the cross-calibration between MSSL OGSE and Supplier's optical tester.

Note 3) The 18 x 18 mm area is divided into 8 x 8 sections and the PHDs are measured separately in each section.

Note 4) Maximum voltages are applied individually for more than 30min. The remaining voltages are kept at nominal during the test.

Table Sp-1. Operating Voltage Distribution

	Photo-cathode Gap	Voltage across MCP1 + MCP2	Anode Gap Voltage
Nominal	350V	2000-2700	4500-5500

Table 1_2. Production history of FM intensifiers from DEP

	DEP's S/N	MSSL's S/N	Note
1st batch	F804502	DEP_#1	FM primary
6 March '98	F804501	DEP_#2	donated by DEP

2nd batch	F813105	DEP_#4	FM secondary
21 April '98	F813101	DEP_#5	Filed trial
3rd batch	F813104	DEP_#6	FM spare #1
19 Jun '98	F813102	DEP_#7	FM spare #2
4th batch		DEP_#8	ruggedness test
21 Dec '98			

---

2. Resolution

The resolution of the XMM-OM detector, employing proximity gap focusing, depends on the wavelength of an input photon and the photocathode gap of an individual intensifier. Since the resolution is expected to be worse at UV wavelengths, a very narrow photocathode gap, 150um, was specified for the FM-intensifiers. The Photocathode gaps among the FM intensifiers were, however, revealed to be different, by the resolution tests at UV wavelengths.

The resolutions of the two FM intensifiers were measured only at 460nm and 630nm but not at UV wavelengths (the most crucial region) to meet the tight FM schedule. As an alternative, the behaviour of resolution versus wavelength was characterized with other spare intensifiers. The resolutions of the two FM intensifiers at UV wavelengths were estimated from these data.

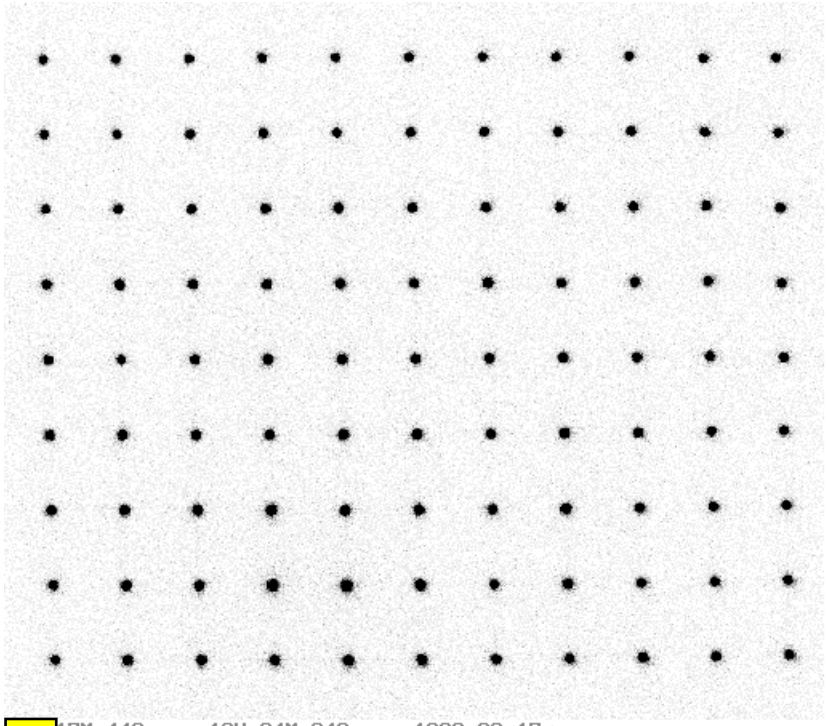

Pinhole array image for resolution test at visual wavelengths

17M 44S 13H 34M 24S 1998/03/17/
22 Res Blue 1000S CCD=(65,17) (1678,1039) 397-2200-4950 DEP_#1 tube

Fig. 2_1

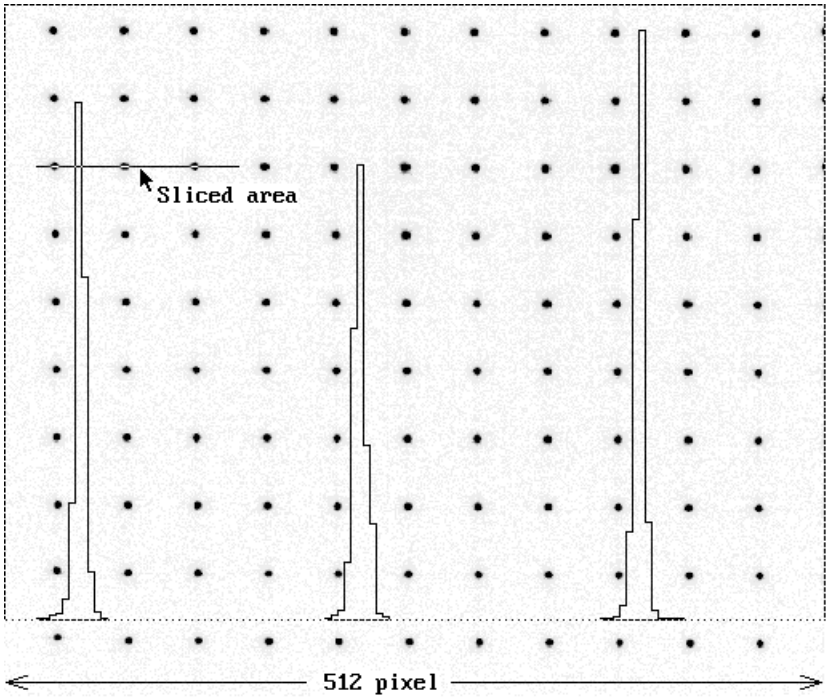

1800 count

Pinhole array image with blue LED

Vc=400V
Nikon 50mm lens

900

0

46M 09S 12H 56M 09S 1998/07/01/
19 Res 460nm 0600S 400-2390-5220 DEP-6

Fig. 2_1B

Two optical set-ups were employed; one for visual wavelengths and the other for UV wavelengths. For the optical set-up (called non-vacuum OGSE), pinhole images were projected on an intensifier using Nikon 50mm printing lens in visual wavelengths (see Fig. 2_1 for DEP_#1 tube and Fig. 2_1.b for DEP_#6 tube). The pinhole image size on the detector is smaller than 6um. The pinhole images were acquired with 5 different photocathode voltages, Vc=400, 300, 200, 100 and 50 volts, to separate the photocathode gap effect from other effects (i.e. optical aberration, centroiding inaccuracy and off-focusing). The 90- 110 spots, depending on how many pinholes were located within a selection area,

were used for assessing the resolution. Since the detector input window has strong curvature, which causes coma aberration at the boundary of the detector field, the data selection window was placed in the central 4.7mmx4.7mm area. The sizes of the 90-110 spots were measured individually, and the average was calculated (see table 2_1). Blue (centred on 460nm) and red (630nm) LEDs were used for the light sources. All intensifiers were measured with the blue LED, but only DEP_#1, #2 and #6 intensifiers were also measured with the red LED.

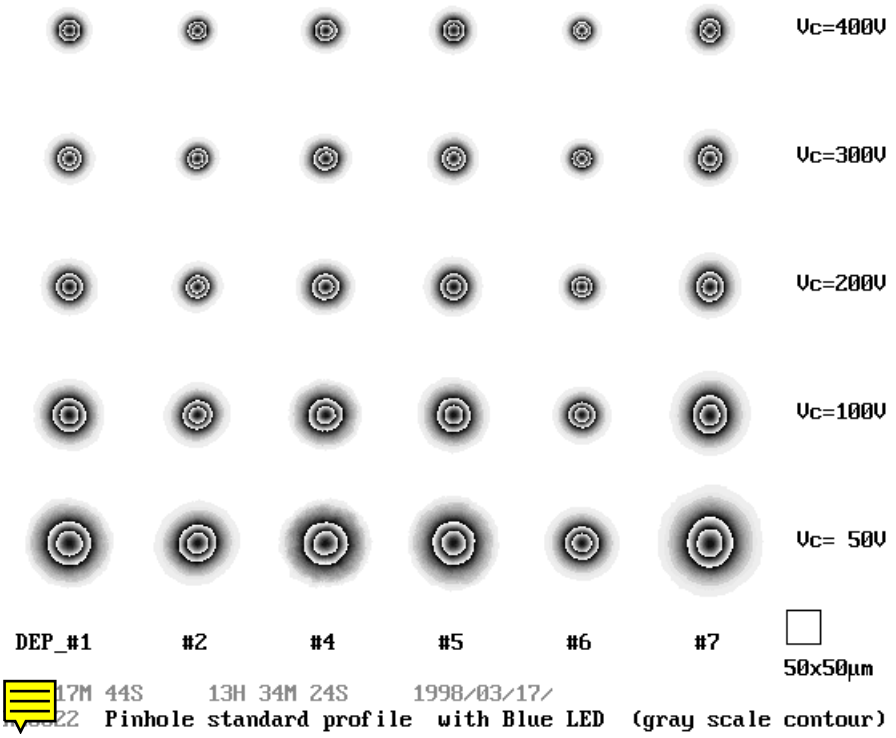

Fig. 2_2

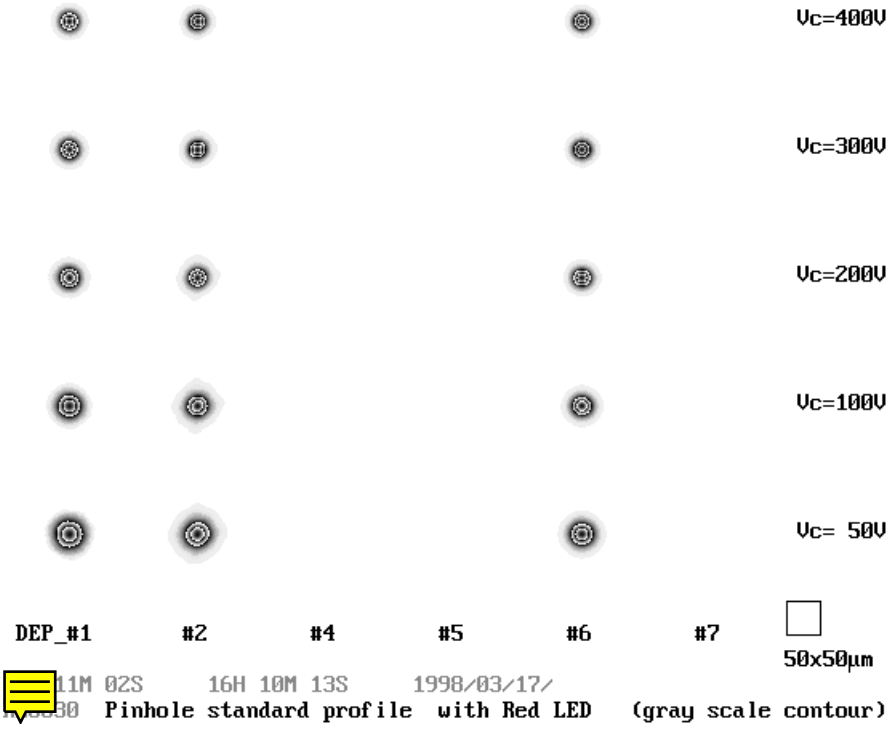

Fig. 2_3

Fig. 2_2 shows standard spot profiles for the blue LED at different photocathode voltages. These were created from the 90-110 pinholes. The difference in resolution among the intensifiers is apparent, specially at the lowest photocathode voltage. The DEP_#7 intensifier shows an elliptical profile (longer along Y-axis). Since the elliptisity is nearly constant throughout the photocathode voltages, this is not due to optical aberration but to a photocathode gap effect. It is not known why the photocathode gap effect is larger along Y-axis than along X-axis. Fig. 2_3 shows standard profile for the red LED. The spot size is smaller. The difference between the intensifiers and with changes in the photocathode voltage are less obvious.

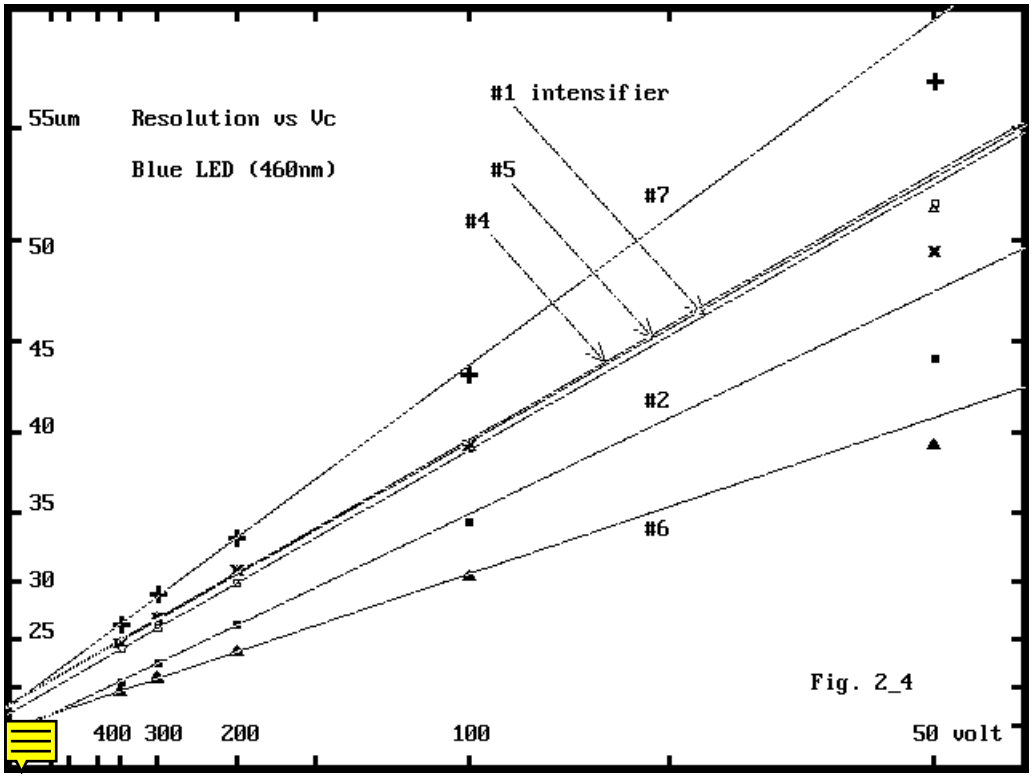

Fig. 2_4

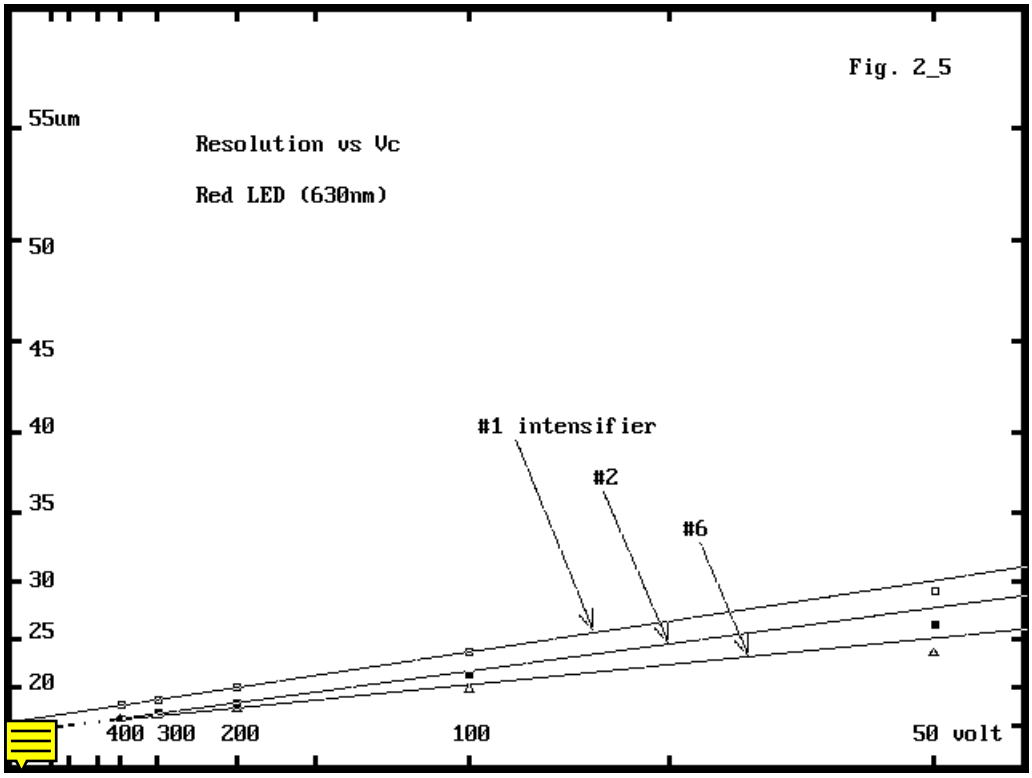

Figures 2_4 and 2_5 show the relationship between resolution and photocathode voltage for the blue LED and for the red LED. The mean of X- and Y- spot widths was used as the representative of resolution, though the spot widths were slightly different between the two axes. The image blurring due to the photocathode gap was quantified from the gradient of the curves and was tabulated in table 2_2. If image blurring due to the photocathode gap is large, the gradient becomes steep. Other effects (i.e. optical aberration, off-focussing, centroiding inaccuracies) shift the curve upward. The ratios of the photocathode effect at 460nm to that at 630nm are tabulated in table 2_3 for the 3 intensifiers. The ratios are extremely similar, in spite of the small effect in visual wavelengths. This may be the benefit of using 100 pinholes.

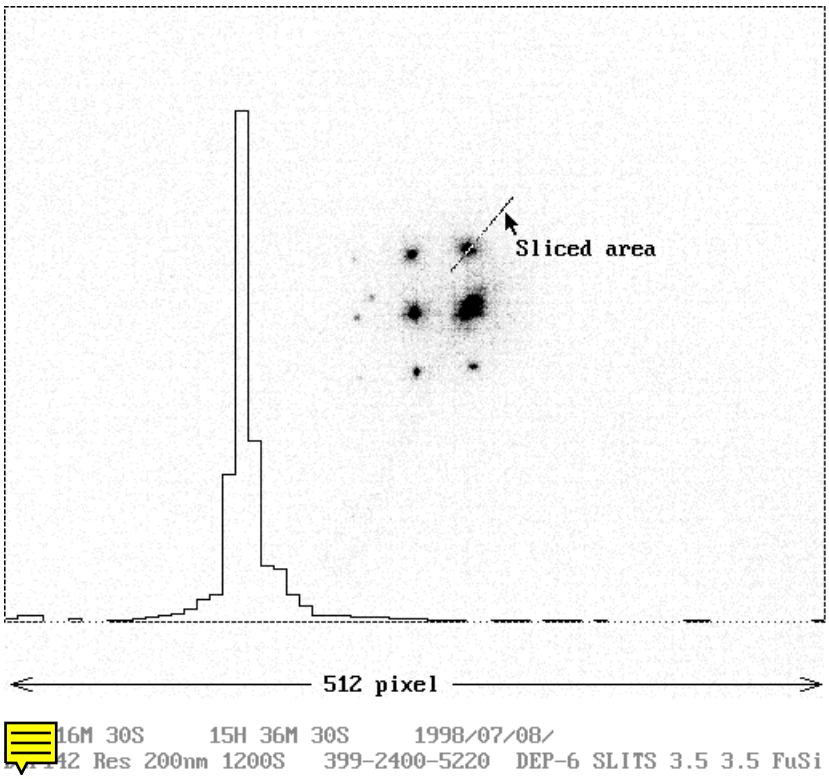

Pinhole image at 200nm with monochrometer

only 3 pinholes were used for the resolution test, because illumination was not uniform

DEP #6 Tube

16M 30S 15H 36M 30S 1998/07/08/
42 Res 200nm 1200S 399-2400-5220 DEP-6 SLITS 3.5 3.5 FuSi F=7.2

Fig. 2_6

The resolution at UV wavelengths was investigated for DEP_#1, #6 and #7 intensifiers using the vacuum monochrometer. The band width of the input light is about 14nm. A 3x3 pinhole array was projected onto the detector using inverse Cassegrain optics (Ealing x15 Reflecting Objective). As the input light beam was collimated but the fine tuning of the direction was not possible inside the vacuum chamber, the illumination of the 9

pinholes was not uniform. Usually only one pinhole was bright. A few pinholes were used for the resolution test, but the 2nd and the 3rd pinholes had low intensities (Figure 2_6).

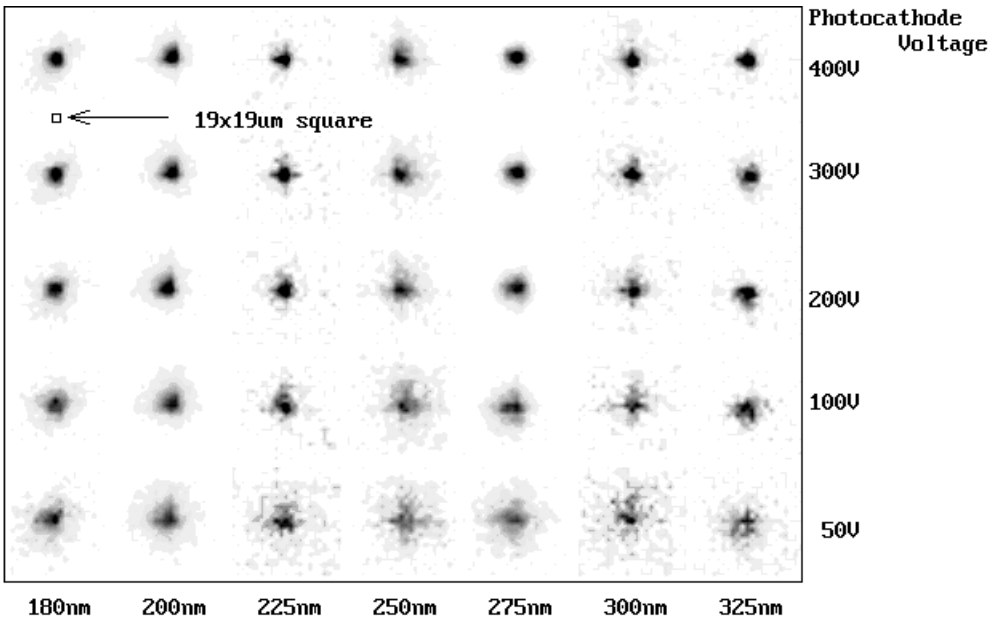

Spot profile v.s. wavelength and photocathode voltage. DEP #6 tube

inal image was magnified by x3 with dithering Fig. 2-7

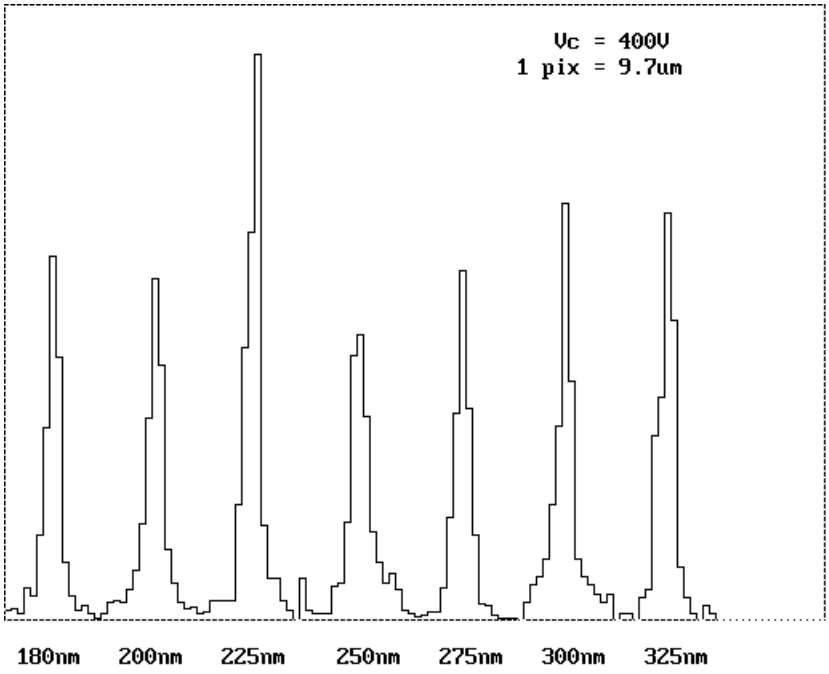

ced profiles of spots at various wavelengths. DEP #6 tube Fig. 2_8

The pinhole images were acquired with 5 different photocathode voltages at 7 wavelengths for the DEP_#6, at 5 wavelengths for the DEP_#2 and at 3 wavelengths for the DEP_#7 intensifier. A pinhole image of the DEP_#6 intensifier located at top right position in Figure 2_6 was examined in detail. Figure 2_7 shows the pinhole image at various wavelengths with different photocathode voltages. The profiles showed non-circular distorted features probably due to optical aberration associated with poor optics alignment. The pinhole width changes with azimuth angle being sliced. The pinhole images, however, were sliced only along X- and Y- directions without adjusting azimuth angle for a systematic

programmable analysis. The height of the slicing strip was 3 sub-pixels. Figure 2_8 shows a slice along the x-direction at the various wavelengths with Vc=400V.

As the UV monochrometer optics are not as good as that for visual wavelengths, the pinhole width in a raw image alone does not tell much about the true resolution of the intensifier. The measured pinhole width varies pinhole by pinhole and azimuth angle of slice. This may be due to coma aberration of optics related to different light beam widths caused by the non-uniform illumination. The spot size of a raw image was represented by the best resolution among the pinholes and along X- or Y-directions (table 2_1), as the larger spot was believed to be the result of the optical aberration. It should be noted that a different rule was applied to express raw spot size in UV wavelengths and in visual wavelengths. In the latter case, the raw spot size was represented by the average of X- and Y-width of 100 spots.

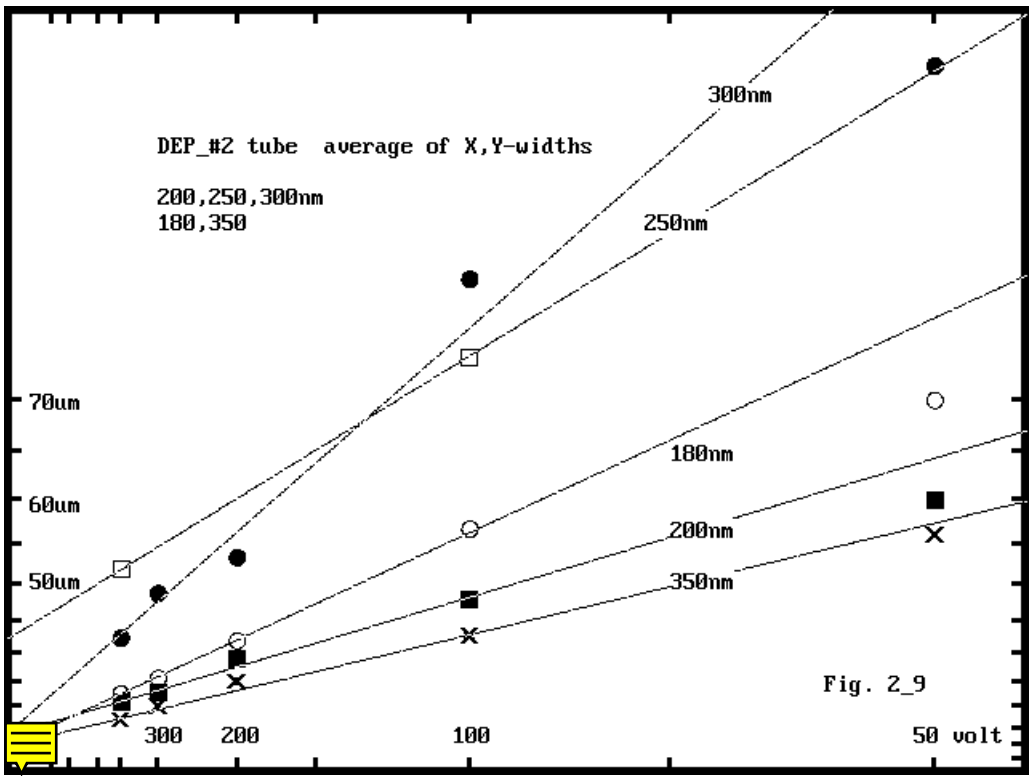

Fig. 2_9

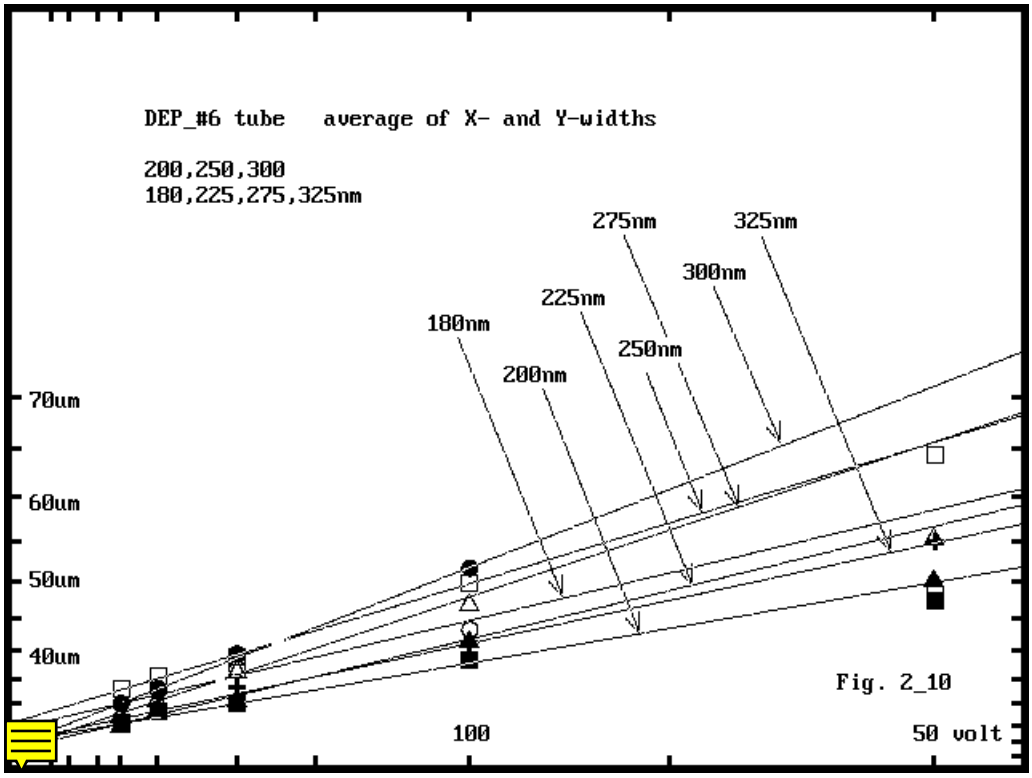

Fig. 2_10

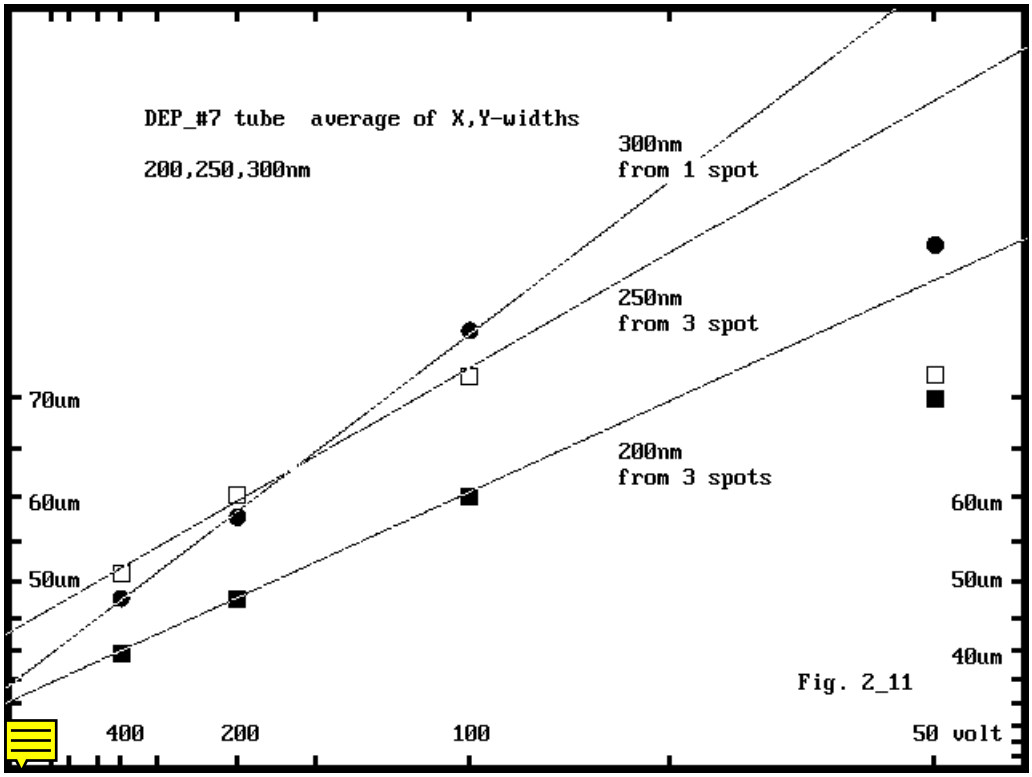

Fig. 2_11

Figures. 2_9, 2_10 and 2_11 show the relation of the spot size versus photocathode voltage at various wavelengths for DEP_#2, #6, #7 intensifiers. The image blurring due to the photocathode gap was derived from the gradient of the curves, which were optical aberration free in theory. The results are tabulated in table 2_2. The ratio of the photocathode effects at various wavelengths to that at 460nm is tabulated in table 2_3.

The most accurate results were obtained with DEP_#6 intensifier, because the pinhole images were sharp

at all wavelengths and all photocathode voltages. While the worst ones were with DEP_#7 intensifier because pinhole images were diluted, particularly at the lower photocathode voltages at 300nm. In terms of wavelength, the best results were at 200nm, as the pinhole widths were small for all intensifiers. The number of pinholes used in the analysis is tabulated in table 2_4, which gives an idea of the accuracy of the results. The photocathode gap effect for the two FM intensifiers, whose resolutions were not measured at UV wavelengths, were estimated from the results of the 3 intensifiers at 200nm, 250nm and 300nm, from DEP_#6 at 180nm, 225nm, 275nm and 325nm, and from DEP_#2 at 350nm. The estimated image blurring is tabulated in table 2_2. Overall spot size in a true image is the convolution of the photocathode gap effect and centroiding inaccuracy. The centroiding inaccuracy for DEP_#1 and DEP_#4 intensifiers were empirically determined from the cross section of the fitted line with Vc=infinity in Fig 2_4 (Blue LED resolution test), though there may still be small effects from optical aberration. The centroiding error is 17um for DEP_#1 and 17.5um for DEP_#4. The overall spot sizes were calculated for various wavelengths, and are shown in Fig. 2_12 and tabulated in table 2_1. The spot size is larger than 35um around 300nm, which is a problem with the two FM intensifiers. Only DEP_#6 intensifier has excellent resolutions at all wavelengths.

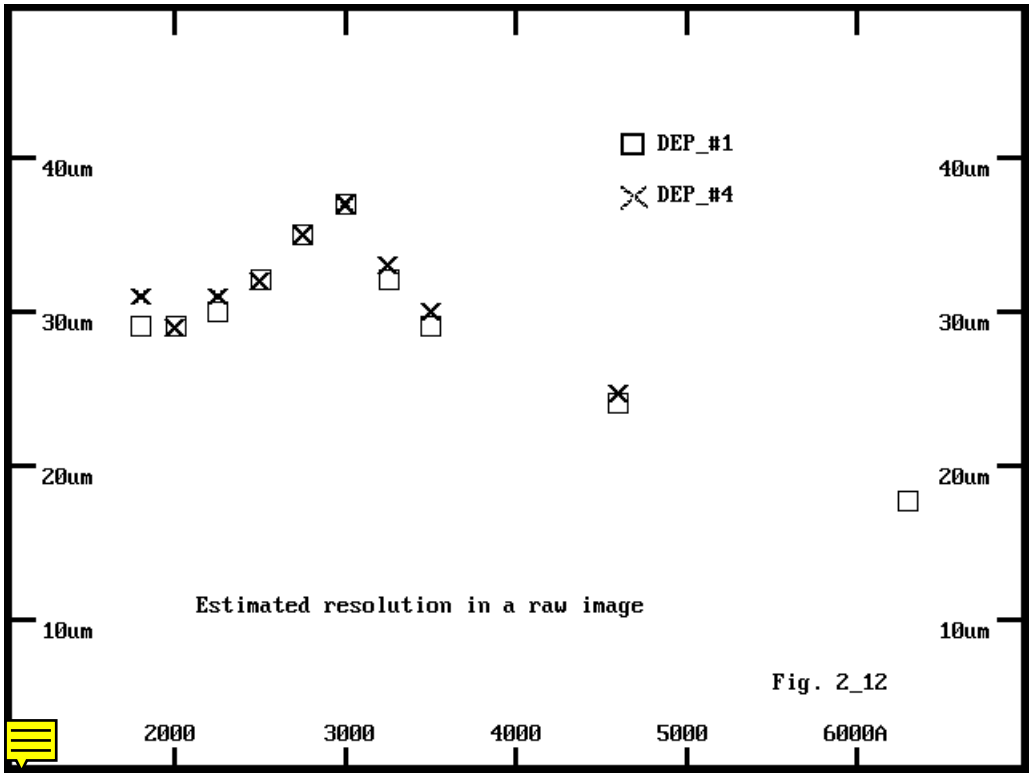

Fig. 2_12

Table 2_1. Spot size in raw image

	DEP_#1	DEP_#2	DEP_#4	DEP_#5	DEP_#6	DEP_#7

Non-vacuum OGSE

630nm	17.6um	15.8um			15.8um	
460nm	24.0um	20.5um	24.7um	24.7um	19.4um	26.2um
Monochrometer						
350nm	(29um?)	24.8um	(30um?)			
325nm	(32um?)		(33um?)		20.7um	
300nm	(37um?)	36.4um	(37um?)		23.7um	46.6um
275nm	(34um?)		(35um?)		22.5um	
250nm	(32um?)	39.7um	(32um?)		23.5um	38.9um
225nm	(30um?)		(31um?)		18.5um	
200nm	(29um?)	26.4um	(29um?)		19.1um	33.0um
180nm	(29um?)	28.3um	(31um?)		24.7um	

Vc=400V

Table 2_2. Image blurring due to photocathode gap

	DEP_#1	DEP_#2	DEP_#4	DEP_#5	DEP_#6	DEP_#7

Non-vacuum OGSE						
630nm	9.24um	8.44um			7.08um	
460nm	17.7um	16.3um	18.2um	18.1um	13.5um	20.2um
Monochrometer						
350nm	(24um?)	21.9um	(24um?)			
325nm	(27um?)	(28um?)	20.5um			
300nm	(33um?)	33.4um	(33um?)		24.4um	33.6um

275nm	(29um?)		(30um?)	22.6um	
250nm	(27um?)	30.4um	(27um?)	21.4um	21.8um
225nm	(25um?)		(26um?)	19.0um	
200nm	(23um?)	21.5um	(23um?)	16.4um	26.5um
180nm	(24um?)	26.6um	(25um?)	18.4um	

---

estimation for Vc=400V

Table 2_3. Ratio of photocathode gap effect relative to 460nm

---

	DEP_#1	DEP_#2	DEP_#4	DEP_#5	DEP_#6	DEP_#7
Non-vacuum OGSE						
630nm	0.5220	0.5178			0.5244	
460nm	1.000	1.000	1.000	1.000	1.000	1.000
Monochrometer						
350nm	{1.34}	1.344	{1.34}			
325nm	[1.52]		[1.52]		1.519	
300nm	(1.84)	2.049	(1.84)		1.807	1.663
275nm	[1.67]		[1.67]		1.674	
250nm	(1.51)	1.865	(1.51)		1.585	1.079
225nm	[1.41]		[1.41]		1.407	
200nm	(1.28)	1.319	(1.28)		1.215	1.312
180nm	[1.36]	1.636	[1.36]		1.363	

Table 2_4. Number of pinhole spots used for analysis

	DEP_#1	DEP_#2	DEP_#4	DEP_#5	DEP_#6	DEP_#7
Non-vacuum OGSE						
630nm	91	90			108	
460nm	92	90	100	92	110	118
Monochrometer						
350nm	2					
325nm					2	
300nm		1			3	1
275nm					3	
250nm		3			3	3
225nm					2	
200nm		6			3	3
180nm		1			3	

Ref-2 Files used for this section

/depfm1/zdep011.dat - zdep018.dat (blue LED)

zdep022.dat - zdep027.dat (blue LED)

zdep030.dat - zdep034.dat (red LED)

/depfm2/zdep209.dat - zdep213.dat (blue LED)

zdep221.dat - zdep225.dat (red LED)

/depfm4/zdp4003.dat - zdp4007.dat (blue LED)

zdp4011.dat - zdp4012.dat (blue LED)

/depfm5/zdp5008.dat - zdp5013.dat (blue LED)

/depfm6/zdep119.dat - zdep123.dat (blue LED)

zdep125.dat - zdep129.dat (red LED)

/depfm7/zdep130.dat - zdep134.dat (blue LED)

/picture/res/res_bl.dat (blue resolution results)

res_rd.dat (red resolution results)

/depfm2/zdep037.dat - zdep043.dat (550nm)

zdep044.dat - zdep048.dat (594nm)

zdep049.dat - zdep053.dat (460nm)

zdep054.dat - zdep058.dat (350nm)

zdep060.dat - zdep064.dat (200nm)

zdep065.dat - zdep066.dat (250nm)

zdep079.dat - zdep080.dat (250nm)

zdep067.dat - zdep071.dat (300nm)

zdep072.dat - zdep078.dat (180nm)

/depfm6/zdep142.dat - zdep146.dat (200nm)

zdep149.dat - zdep153.dat (250nm)

zdep158.dat - zdep165.dat (300nm)

zdep169.dat - zdep173.dat (225nm)

zdep176.dat - zdep180.dat (275nm)

zdep183.dat - zdep187.dat (325nm)

zdep190.dat - zdep194.dat (180nm)

zdep256.dat - zdep259.dat (200nm)

/depfm7/zdep232.dat - zdep235.dat (300nm)

zdep236.dat - zdep239.dat (250nm)

zdep243.dat - zdep246.dat (200nm)

zdep250.dat - zdep253.dat (300nm)

/picture/res/resprox.dat (all monochrometer results)

3. Quantum Efficiencies

XMM-OM intensifiers employ S-20 photocathode to cover a wide spectral range, i.e. 1700-6000A. The two FM intensifiers were, however, delivered to ESA without measurement of Q.E.s by MSSL to meet the tight FM

schedule. Their R.Q.E.s (photo-cathode sensitivity) were measured by DEP in the wavelength range of 2000A-9000A during manufacturing. MSSL used DEP's R.Q.E. as an alternative at the time of FM delivery. The R.Q.E.s for all intensifiers are plotted in Figure 3_1. All showed similar sensitivities and clearly higher than specifications (20% @300nm, 6% @550nm).

The D.Q.E. (Detectable Quantum Efficiency, overall sensitivity of a photon counting detector) and R.Q.E. were measured by MSSL with DEP_#6 and DEP_#7 intensifiers in October 1998 (XMM-OM/MSSL/TC/0053). MSSL's R.Q.E. measurements agreed with DEP's ones very well as shown in Fig 3_2. The ratio of D.Q.E. to R.Q.E. was 70% at 2000-5800A for both intensifiers. The difference expands below 2000A, which might be due to enhancement of the R.Q.E. by pair photo-electron emission from the photocathode.

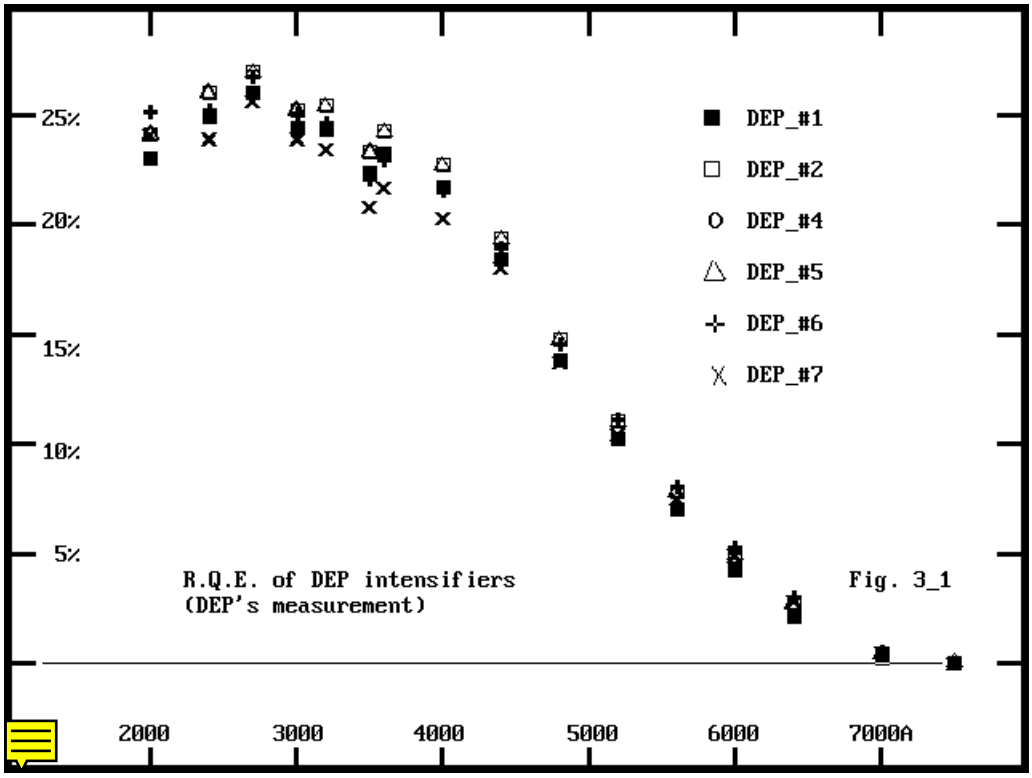

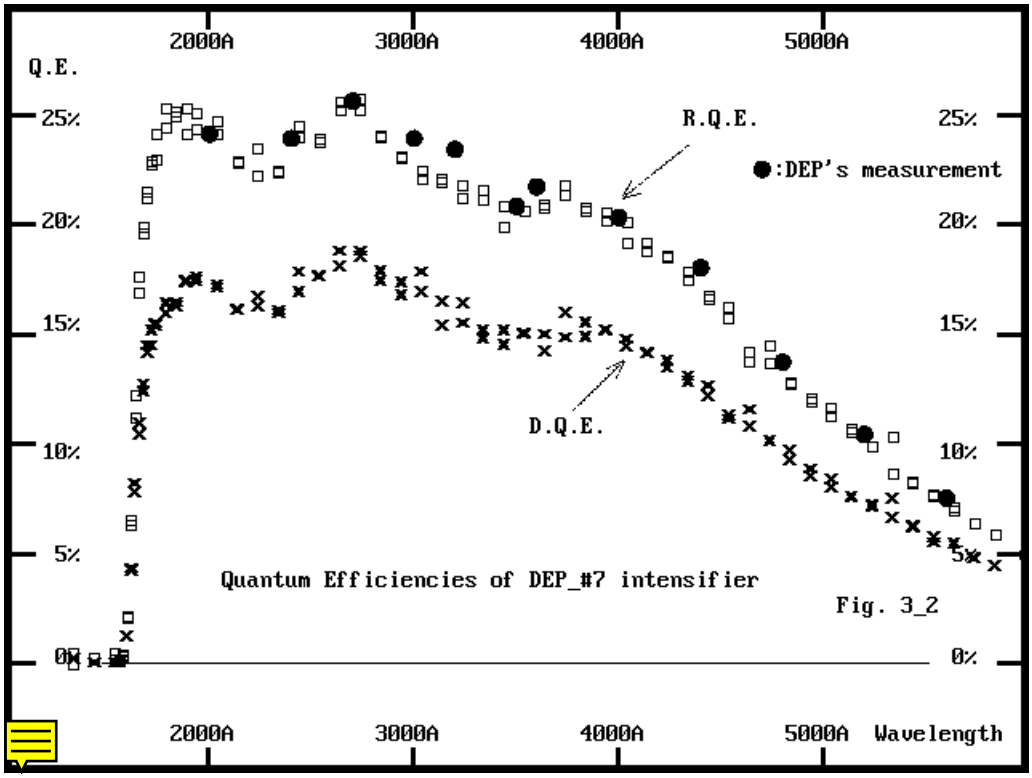

Ref-3 Files used for this section

/picture/qe/rqedep.alk (RQE, DEP's measurement)

/rqetab5.deu (RQE DEP_#6)

/rqetab6.deu (RQE DEP_#7)

/dqetab6.deu (RQE DEP_#6)

/dqetab7.deu (RQE DEP_#7)

4. Dark Current and SW-on channels

A long integration was carried out in photon counting mode with the photocathode-ON under dark conditions (Figures 4_1a, 4_2a, 4_3a, 4_4a and 4_5a). Since the dark file for the DEP_#5 intensifier was deleted by

accident, a F-F image with relatively low illumination is shown in Figure 4_3a as an alternative. The dark current of DEP_#2 was not investigated, because the intensifier has 4 big switched-on channels.

The dark currents were measured after running in the dark for a few days to eliminate effects of fluorescence of the window material and trapped charge within the photocathode. DEP_#1 intensifier has relatively large

dark current, showing a coaxial ring pattern, while the other 4 intensifiers, DEP_#4, _#5, _#6 and _#7, showed outstanding low dark current. DEP_#4, #5 and # 6 intensifiers showed edge emission surrounding 90 -180 degrees. These intensities are tabulated in table 4_1. They do not affect the science data, but may be problem in terms of lifetime. DEP_#5 has 2 bright spots, which disappear when Vc=0. These might be photo-cathode emissions - another sign of danger.

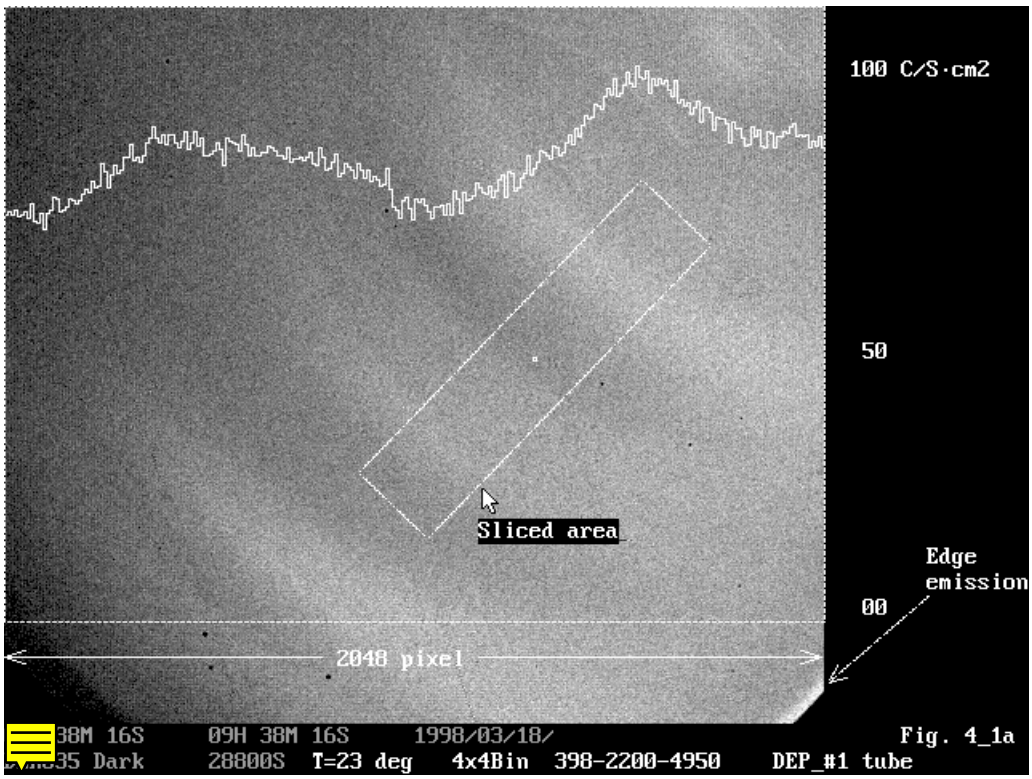

Fig. 4_1a

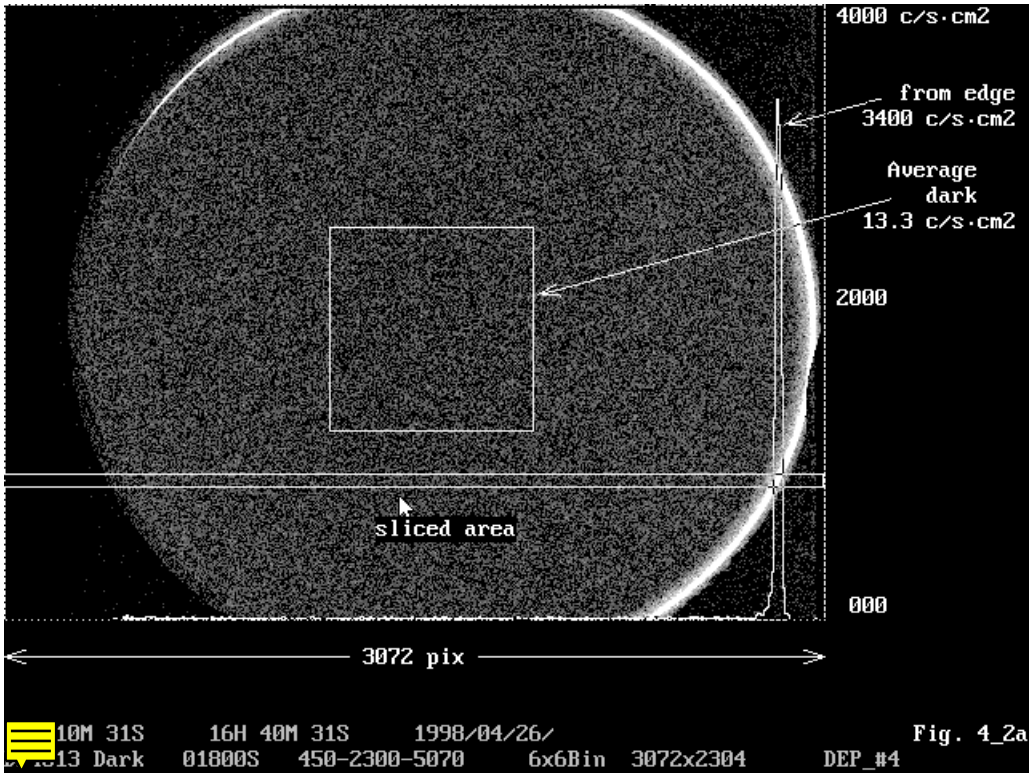

Fig. 4_2a

Fig. 4_3a

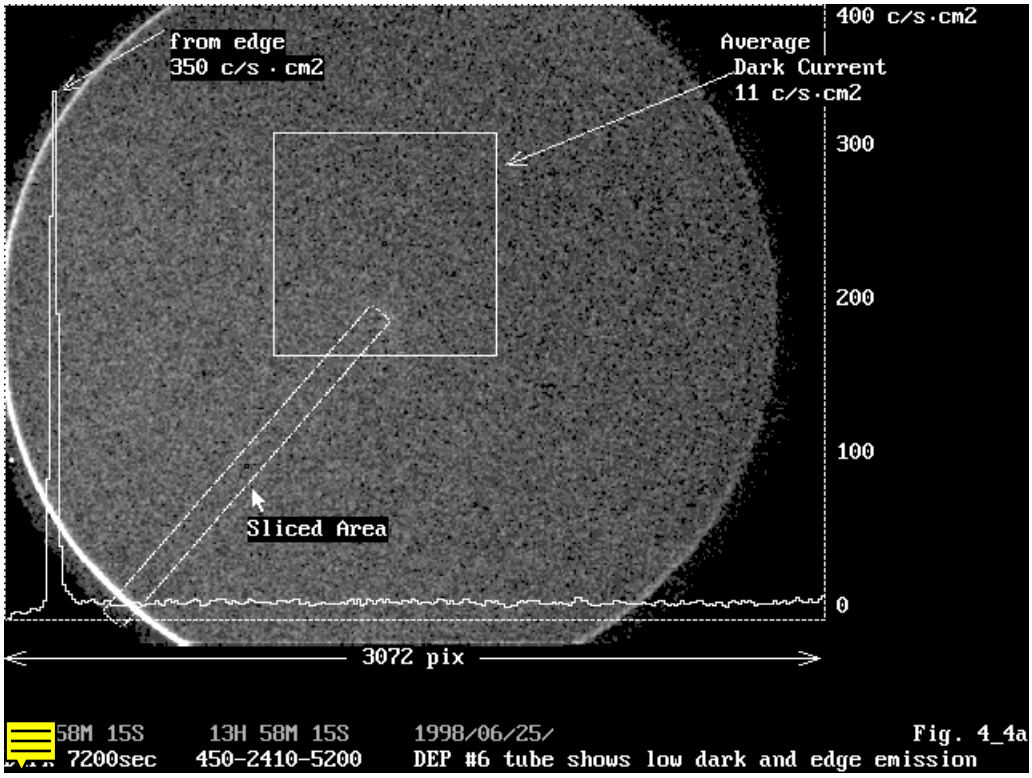

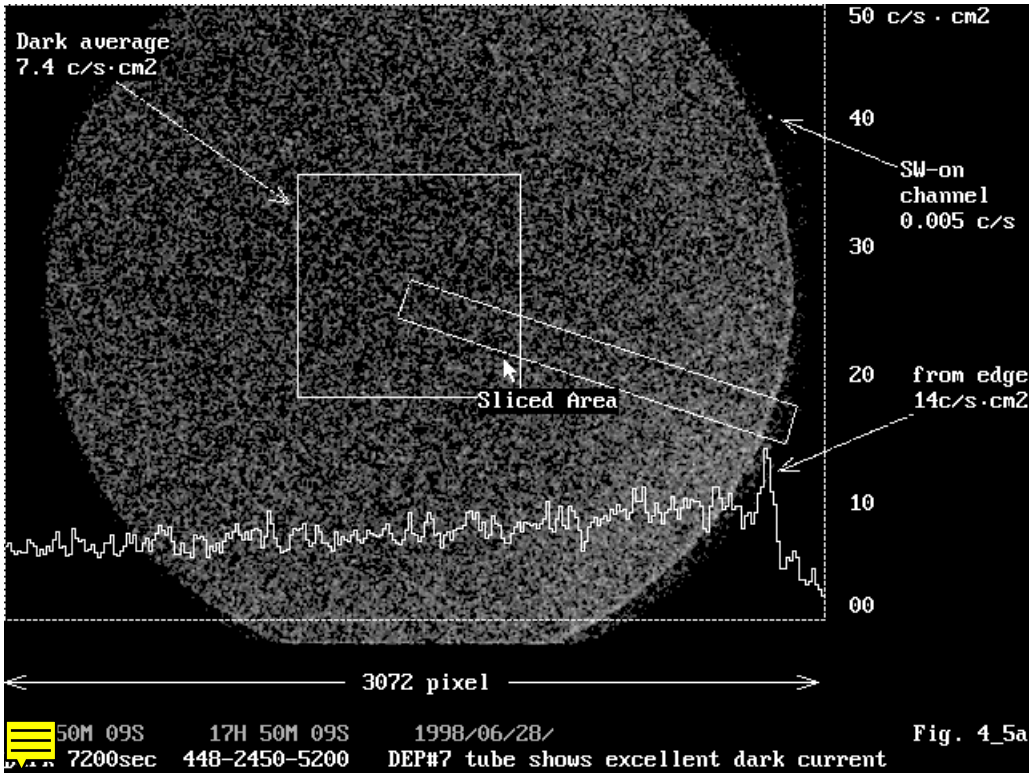

A long integration with photocathode-OFF was also carried out to assess switched-on channels of the MCPs (Figures 4_1b, 4_2b, 4_3b, 4_4b and 4_5b). DEP_#1 intensifier has no noticeable white spots within the

science window, but has some at the edge. The average MCP-dark value is pretty low, 0.24 c/s cm2. DEP_#4 and #6 are extremely clean. There is neither edge emission nor a noticeable bright spot. The average MCP-dark

values are less than 0.5 c/s cm2. DEP_#7 intensifier has some noticeable white spots near the centre and at the edge, but those are far below the specification (0.05 c/s).

DEP_#2 intensifier has very 4 big switched-on channels, which would inhibit its usage in observation. DEP_#5 intensifier has one small switched-on channel. It also shows significant edge emission with Vc-OFF

(see Table 4_1). The edge emission does not affect science data, but may be an indication of danger.

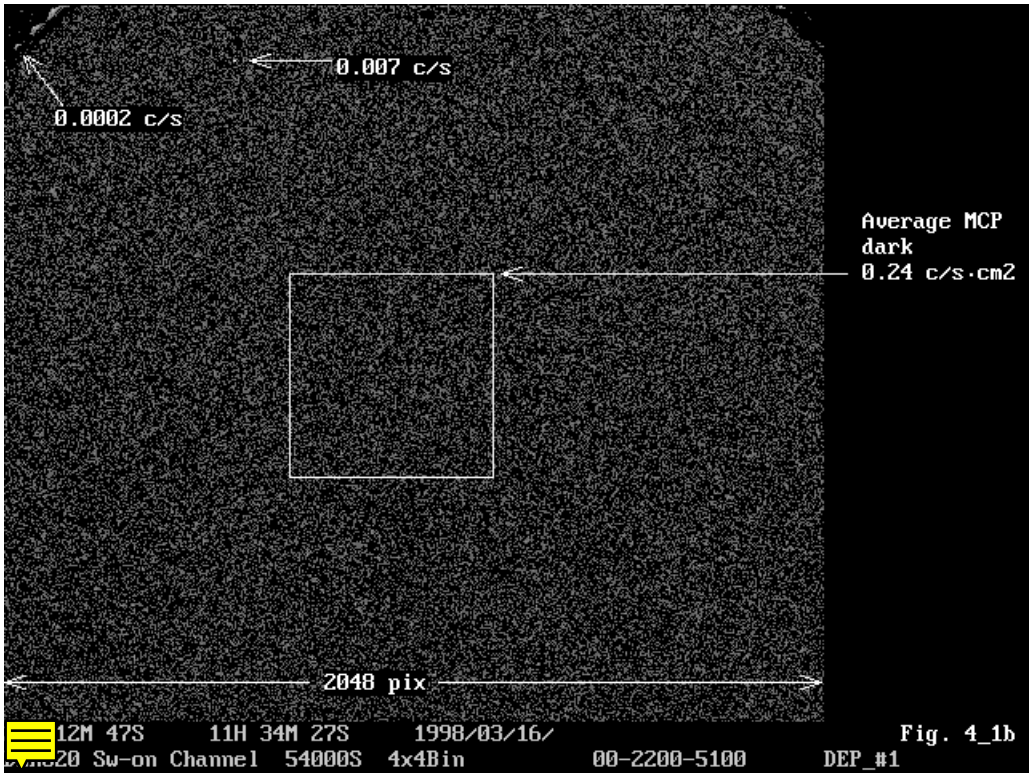

Fig. 4_1b

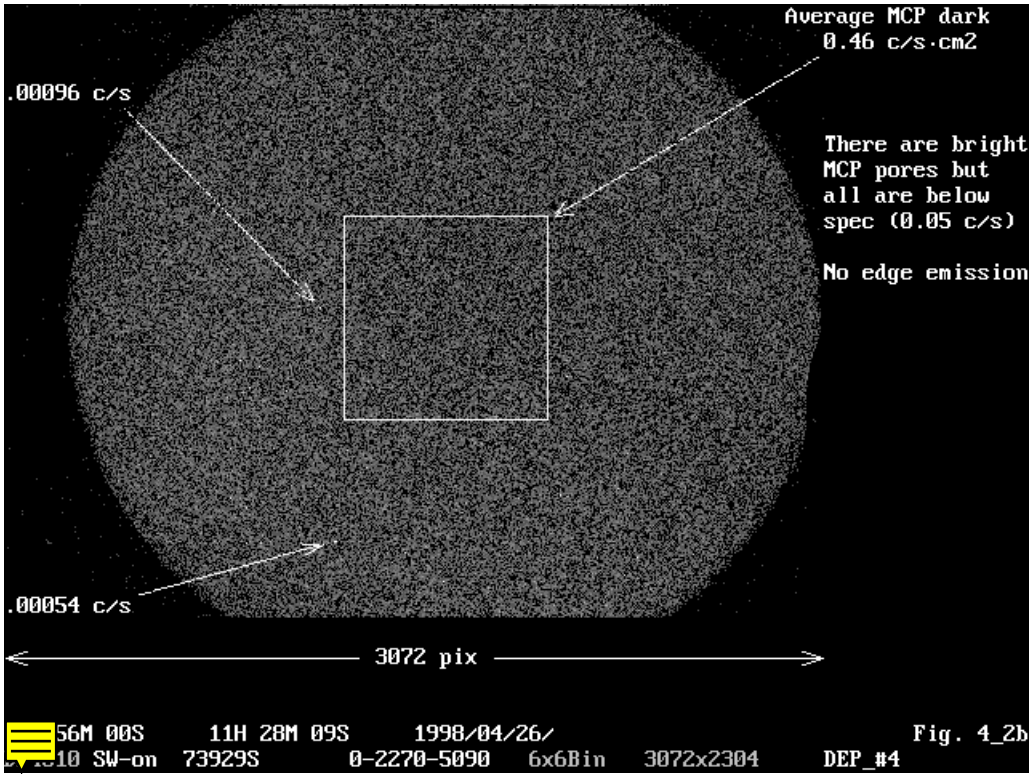

Fig. 4_2b

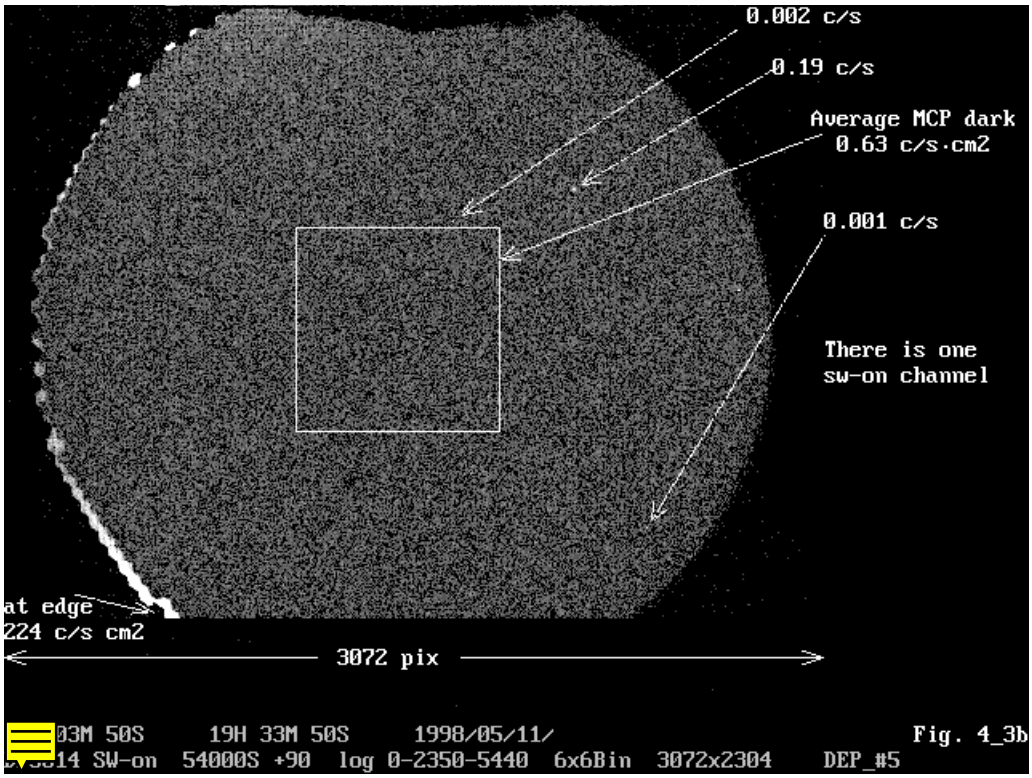

Fig. 4_3b

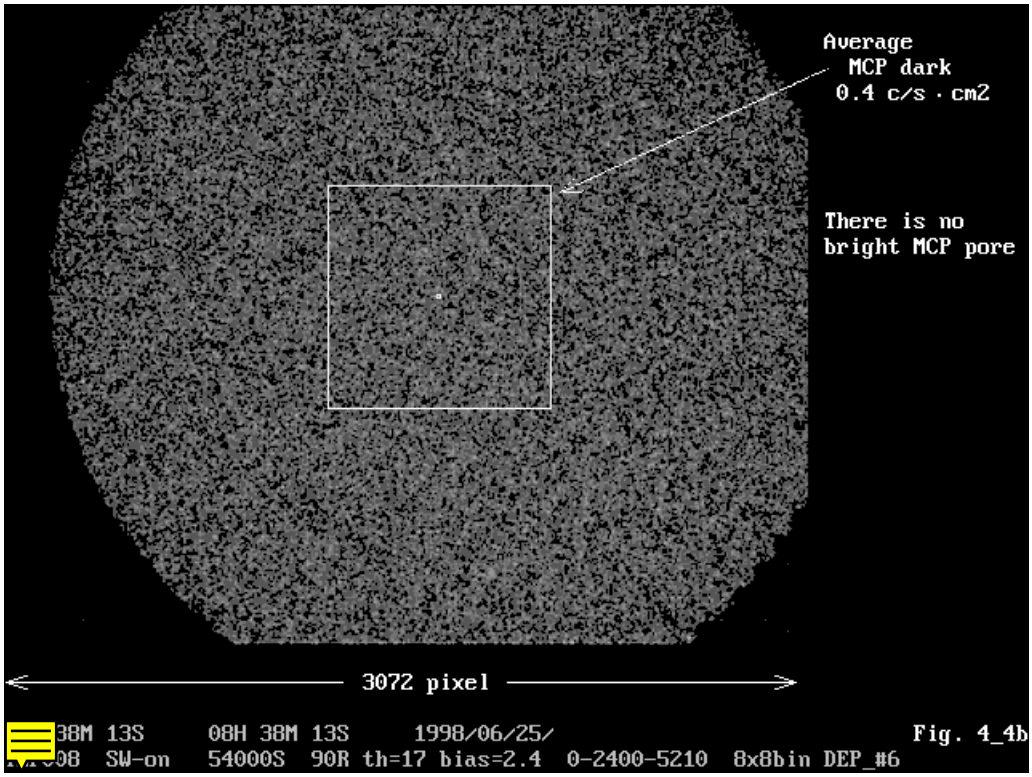

Fig. 4_4b

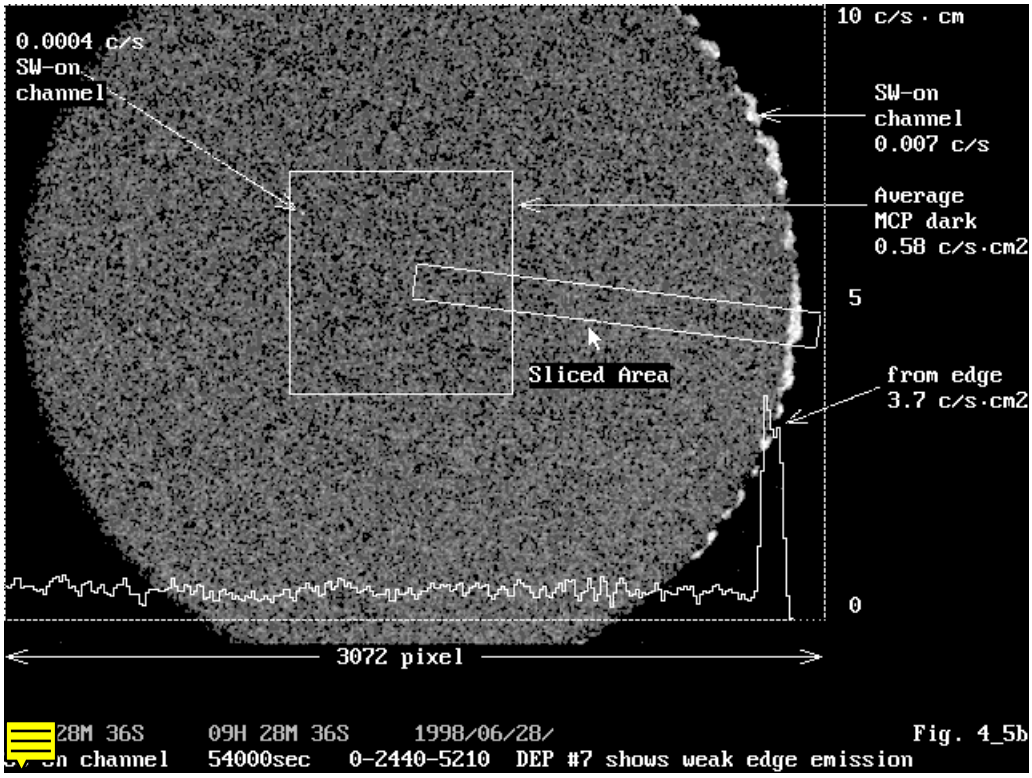

Table 4_1. Dark current

Nominal voltage	DEP_#1	DEP_#2	DEP_#4	DEP_#5	DEP_#6	DEP_#7	DEP_#8
Average Vc-ON	80	---	13.3	10	11	7.4	150 (by DEP)
Average Vc-OFF	0.24	---	0.46	0.63	0.4	0.58	
SW-on channel (>0.05 c/s)	None	Big 4	None	1	None	None	
Edge emission with Vc-ON	70	---	3400	1240	340	7	significantly seen at DEP
Edge emission with Vc-OFF	19	---	None	224	None	3	---

---

unit: counts/(sec cm2)

Ref-4 Files used for this section

/depfm1/zdrk035.dat (dark)

zdrk020.dat (sw-on channel)

/depfm4/zdp4013.dat (dark)

zdp4010.dat (sw-on channel)

/depfm5/zdp5006.dat (faint F-F)

zdp5014.dat (sw-on channel)

/depfm6/jlaf/jlf009.dat (darkF)

jlf008.dat (sw-on channel)

/depfm7/jlaf/jlf003.dat (dark)

jlf001.dat (sw-on channel)

5. Flat Field

Flat field images were acquired in photon counting mode to assess black blemishes in the intensifiers (Figures 5_1a, 5_2a, 5_3a, 5_4a, 5_5a and 5_6a). The blue LED was used as the light source. Sensitivities are quite uniform for the 5 intensifiers. The rms values in the central 4.7mmx4.7mm are tabulated in table 5_1.

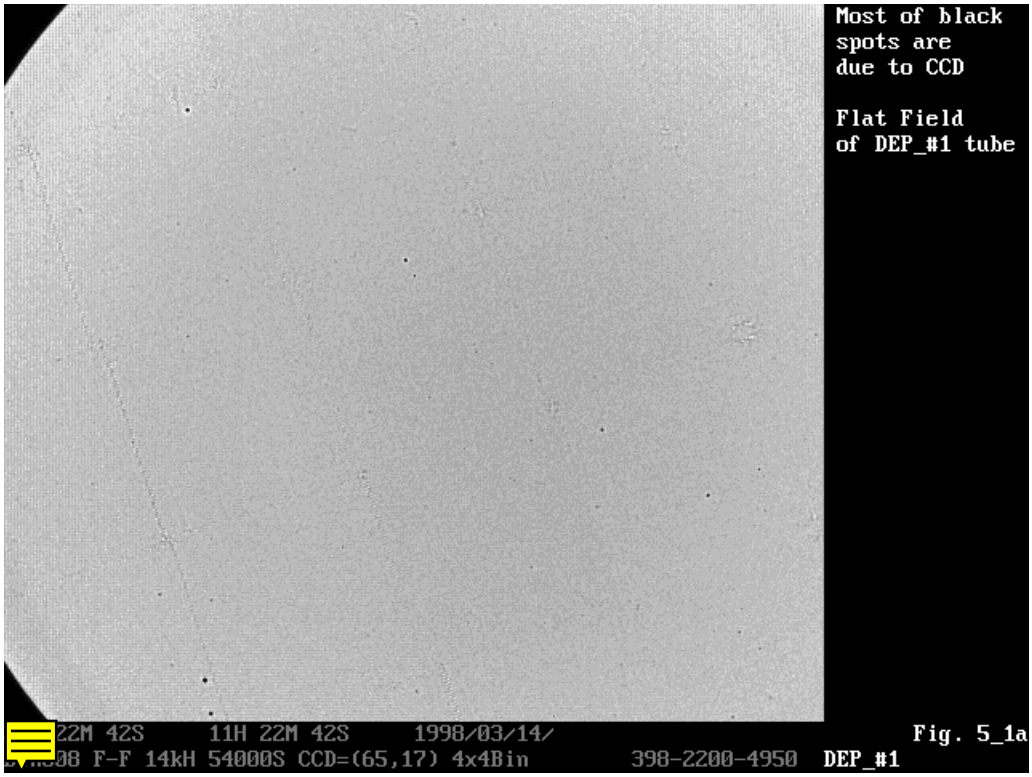

Fig. 5_1a

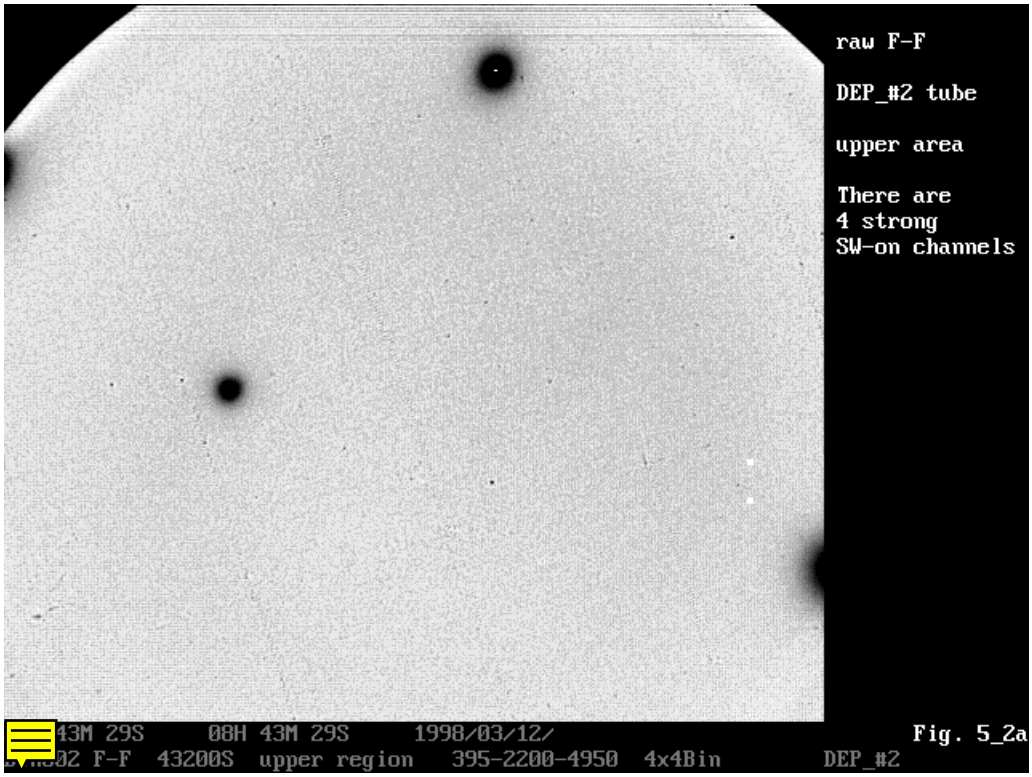

Fig. 5_2a

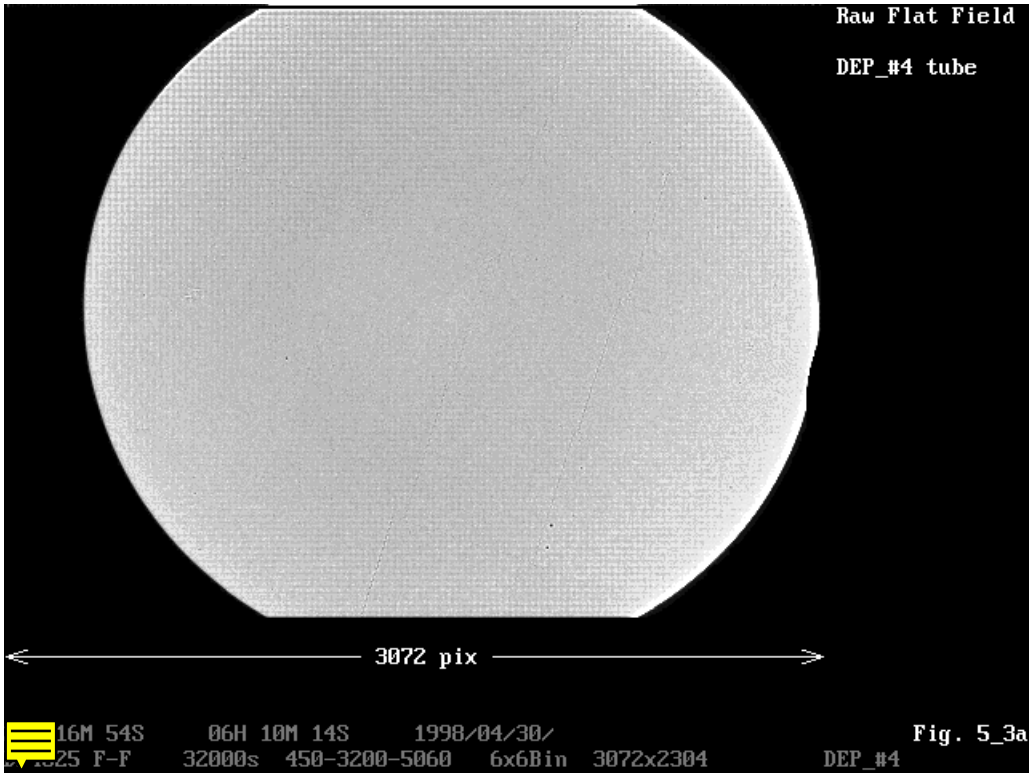

Fig. 5_3a

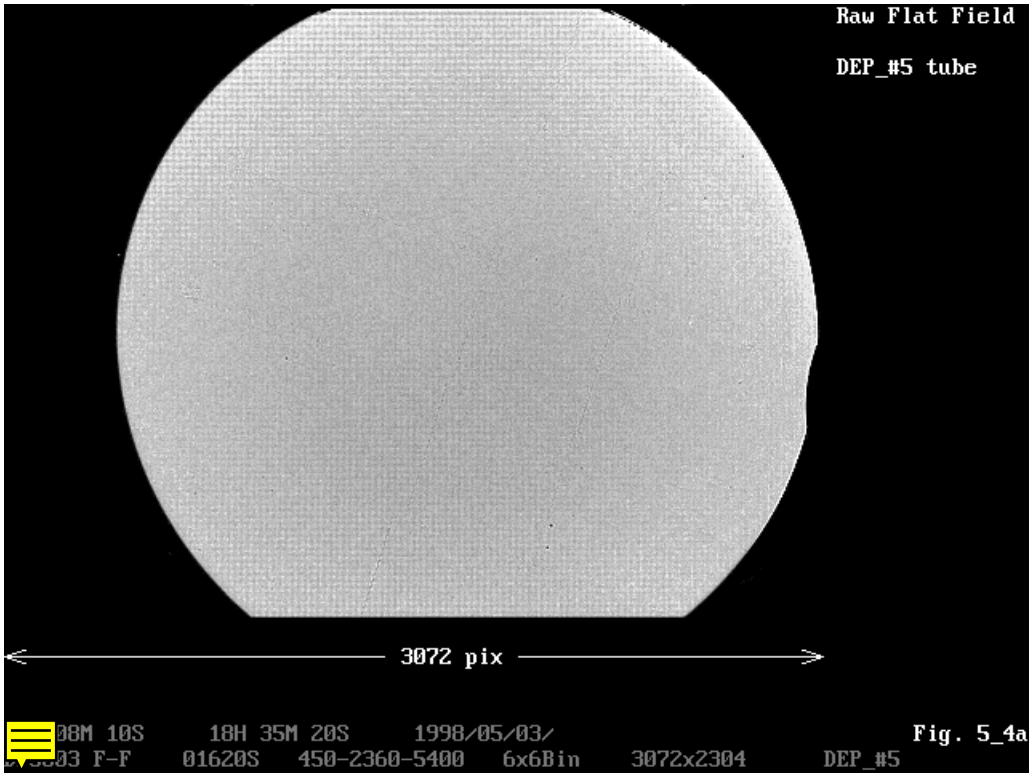

Fig. 5_4a

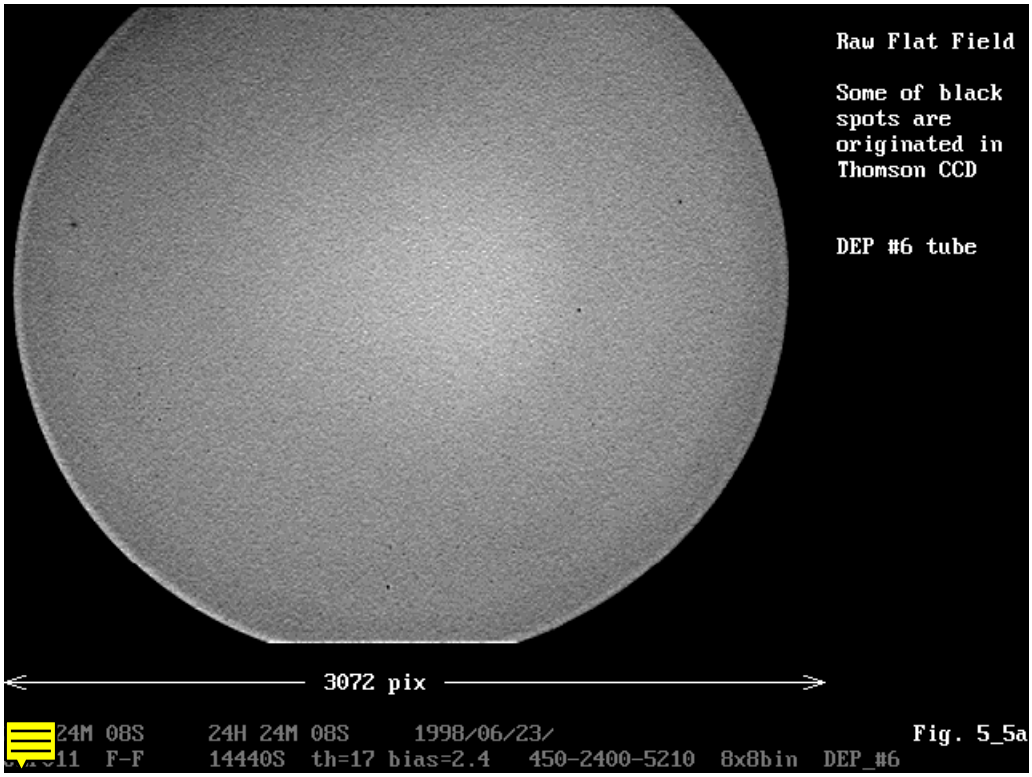

Fig. 5_5a

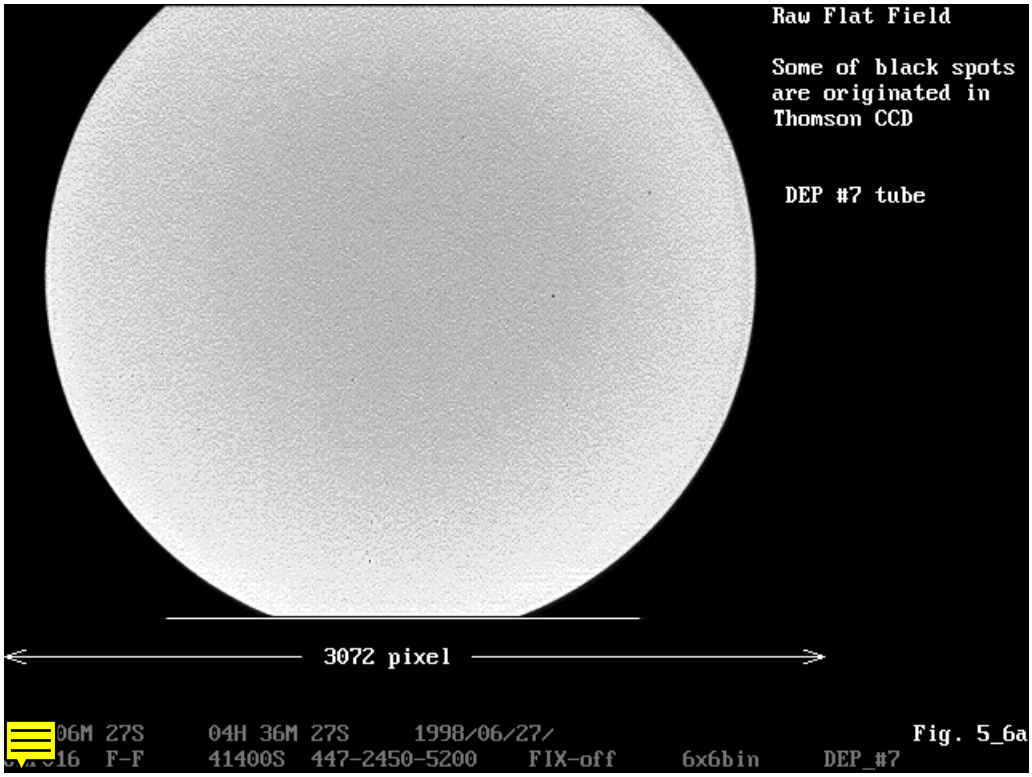

Fig. 5_6a

Most of the black blemishes seen in a raw F-F image are due to the (non-FM) CCD camera. The F-Fs were therefore divided by another F-F image acquired with a different CCD position (i.e. rotating 90 degrees, or

shifting a little). These are shown in Figures 5_1b, 5_2b, 5_3b, 5_4b, 5_5b and 5_6b. The number of black blemishes is tabulated in table 5_1. DEP_#1 intensifier has several tiny (~50um) but deep blemishes within the

2048x2048 science window. DEP_#2 has got the 4 big blemishes due to the switched-on channels, which inhibits the use of this intensifier for observation. DEP_#4 is very clean. DEP_#5 has one deep blemish in the centre of the detector. This intensifier is relatively clean. DEP_#6 intensifier has several blemishes at the 30% level, which are located at the edge of the science window. The #7 intensifier is a little cleaner than DEP_#6. There are several 20% level blemishes near the boundary of the science window.

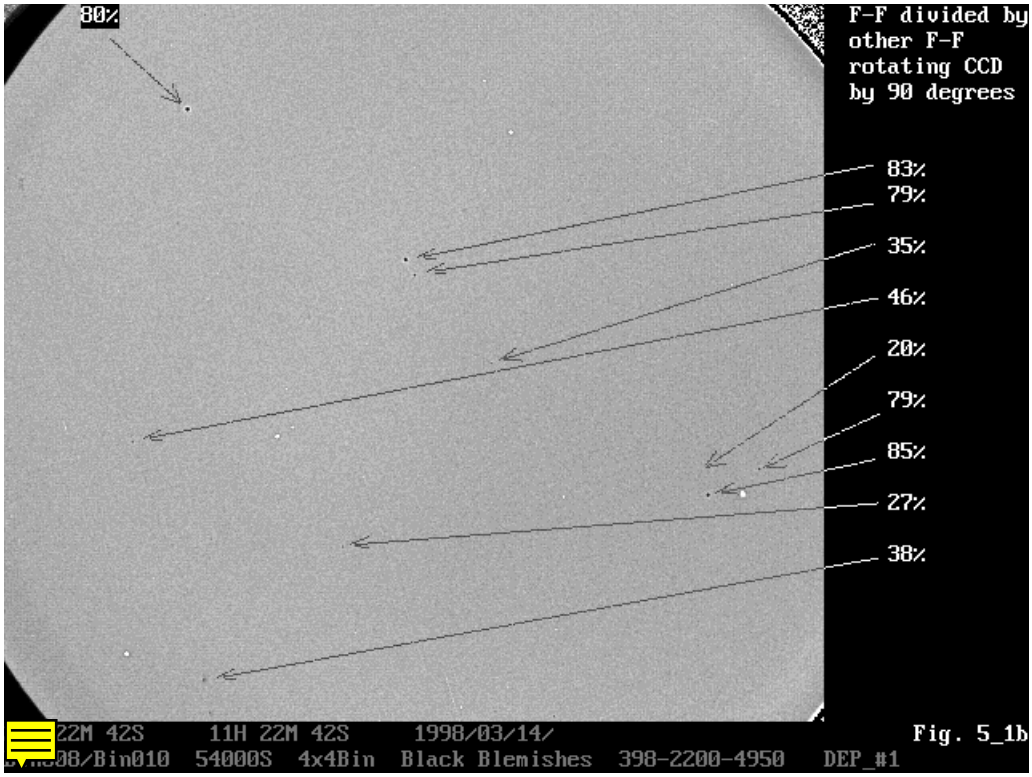

Fig. 5_1b

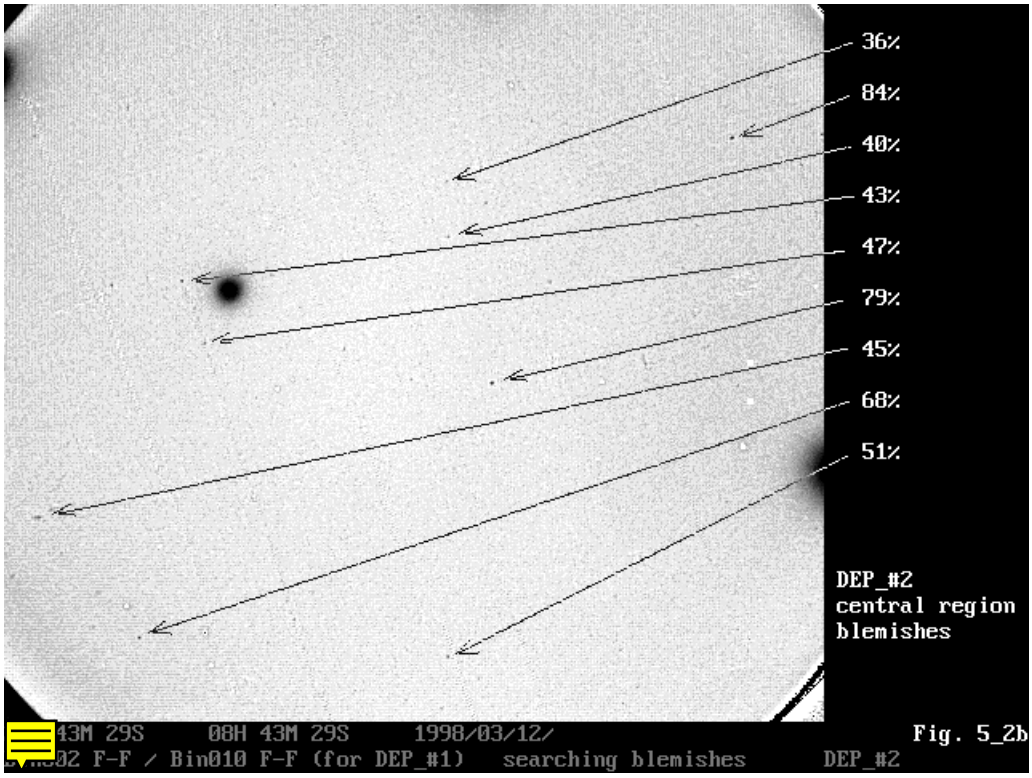

Fig. 5_2b

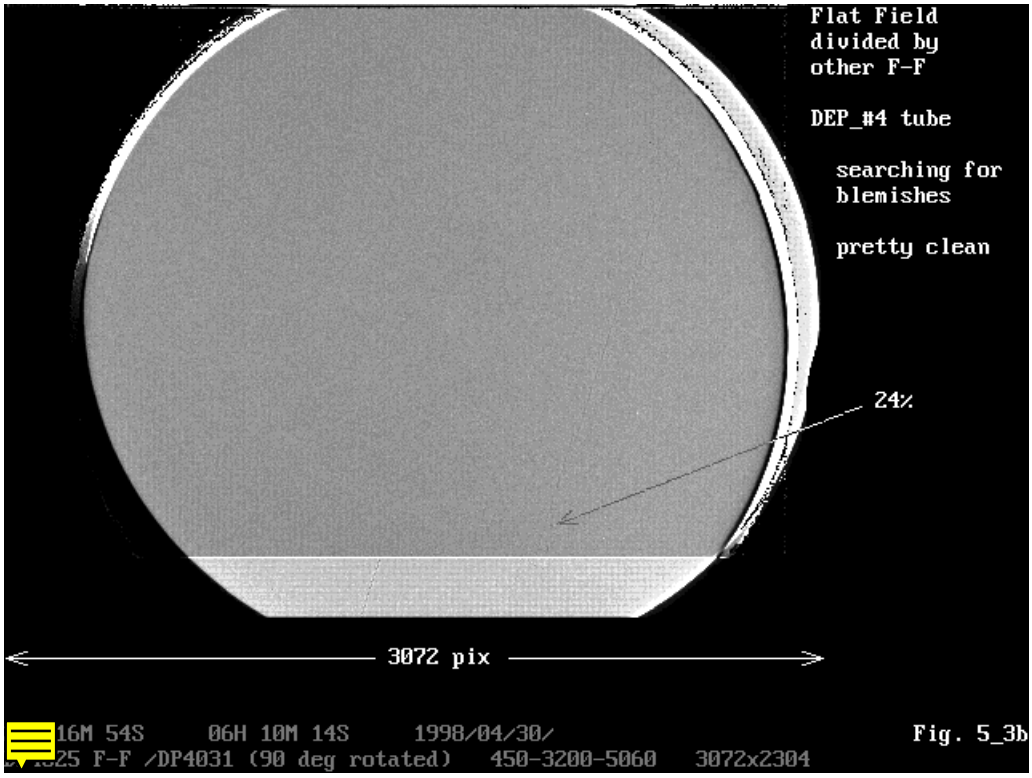

Fig. 5_3b

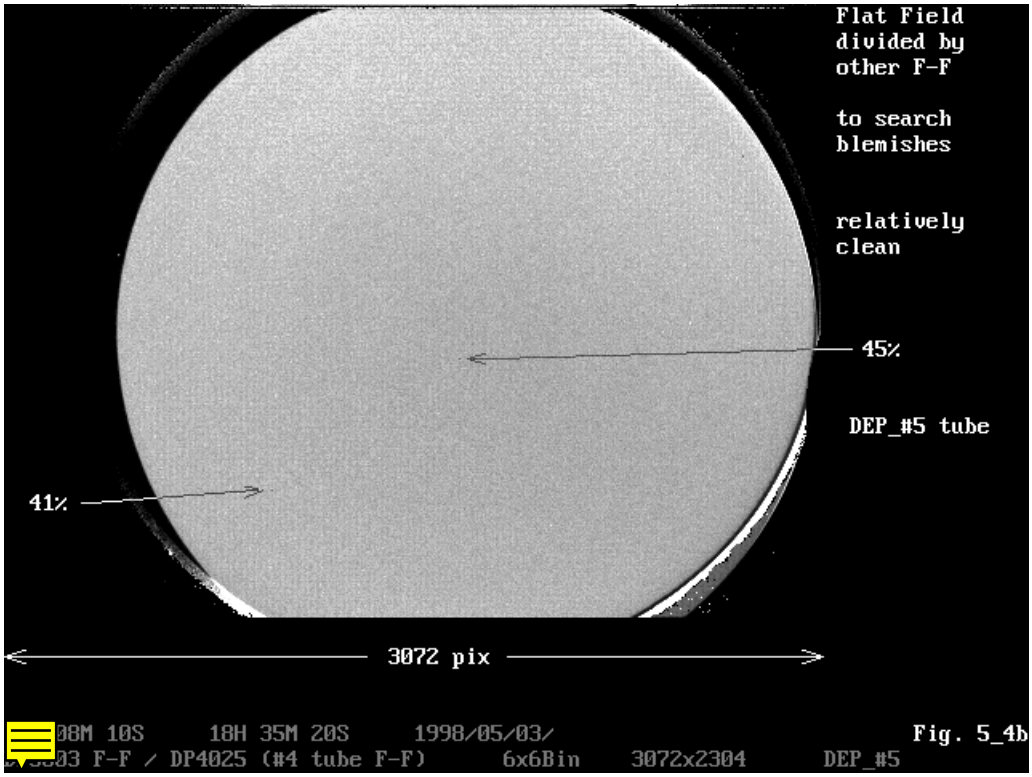

Fig. 5_4b

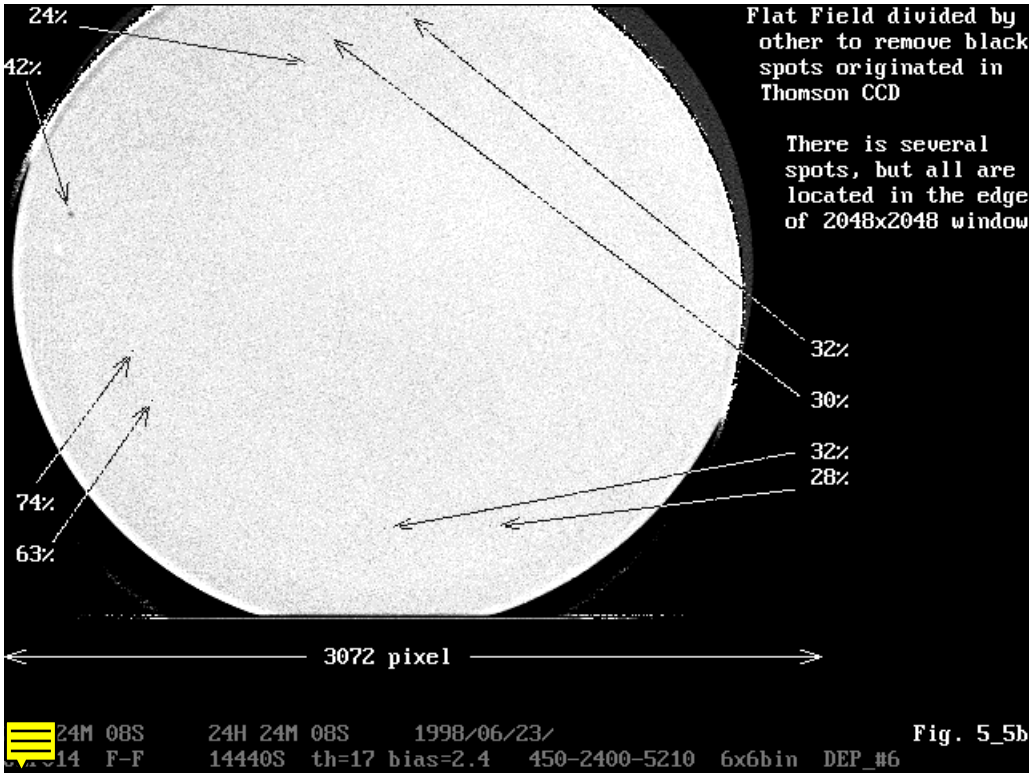

Fig. 5_5b

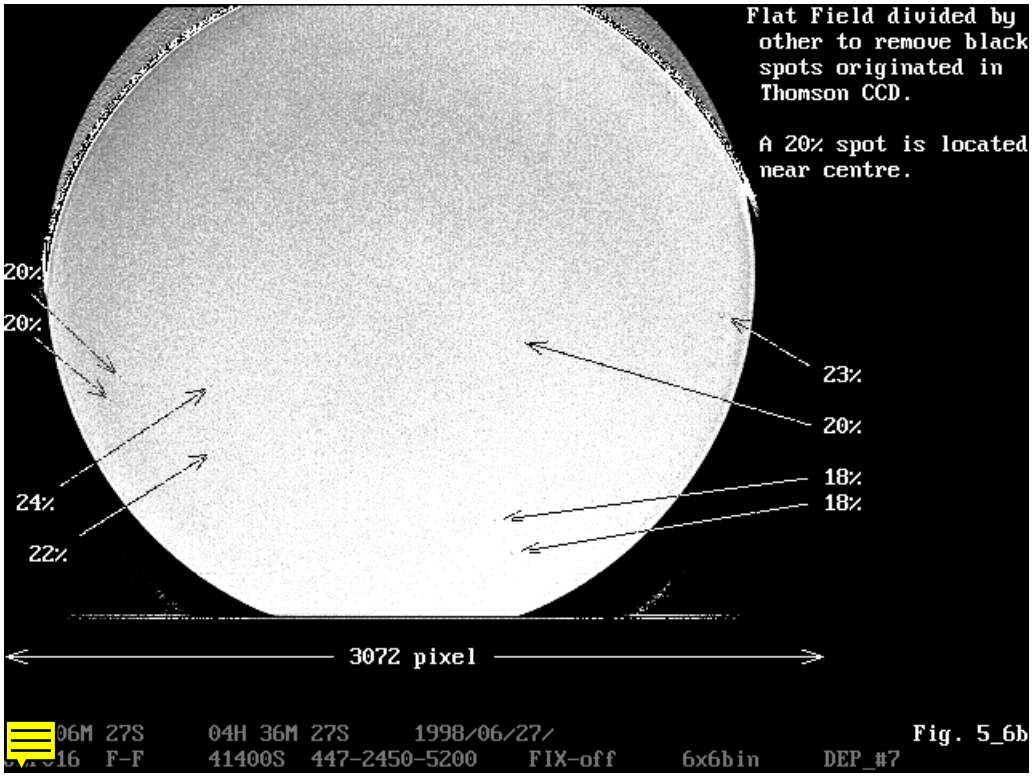

Fig. 5_6b

Table 5_1. Flat field image uniformity

	DEP_#1	DEP_#2	DEP_#4	DEP_#5	DEP_#6	DEP_#7
Rms (%)	3.6	4.3	3.7	5.0	6.4	5.7
No. of black blemishes	10	11	1	2	7	5

Ref-5 Files used for this section

/depfm1/zbin008.dat

zbin010.dat

/depfm2/zbin002.dat

/depfm4/zdp4025.dat

zdp4031.dat

/depfm5/zdp5003.dat

/depfm6/zjlf011.dat

zjlf014.dat

/depfm7/zjlf005.dat

6. Pulse Height Distribution

Figures 6_1, 6_2, 6_3, 6_4, 6_5 and 6_6 show the pulse height distributions of the DEP_#1, #2, #4, #5, #6 and #7 intensifiers. Events are selected from a central 256x256 CCD pixel region. All show relatively broad pulse height distributions, but the broad distributions are compensated by the depth and position of the valley. DEP_#6 shows the best profile among the 6 intensifiers. The characteristics of pulse height distribution are summarized in table 6_1.

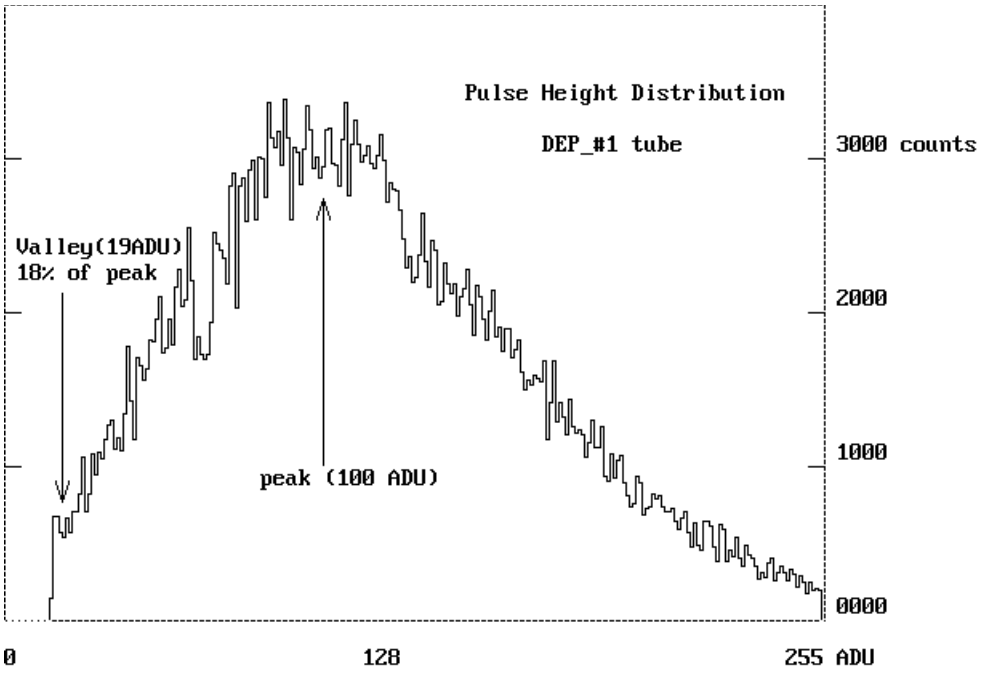

6_1 18H 28M 39S 1998/03/14/
[illegible]06 PHD 2000FR 197956 event CCD=(65,17) 398-2200-4950 DEP_#1

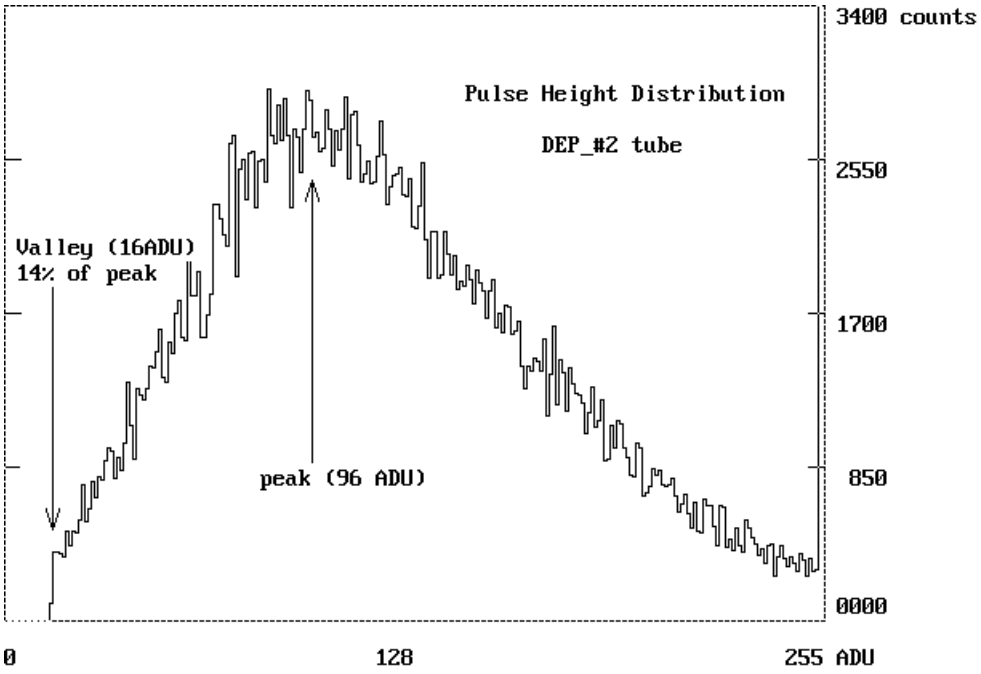

6_2 11H 44M 28S 1998/07/30/
[illegible]08 PHD 1000FR 182101 events TH=15 400-2235-5001 DEP_#2

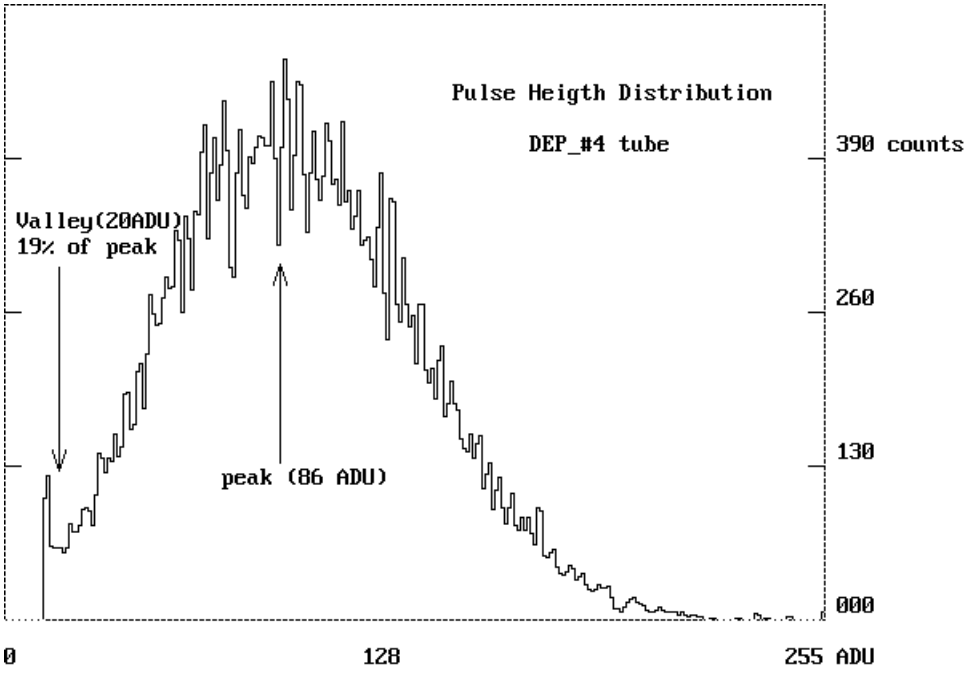

6_3 13H 06M 00S 1998/05/13/
[illegible]8 PHD from PHD004.DAT DEP_#4 tube

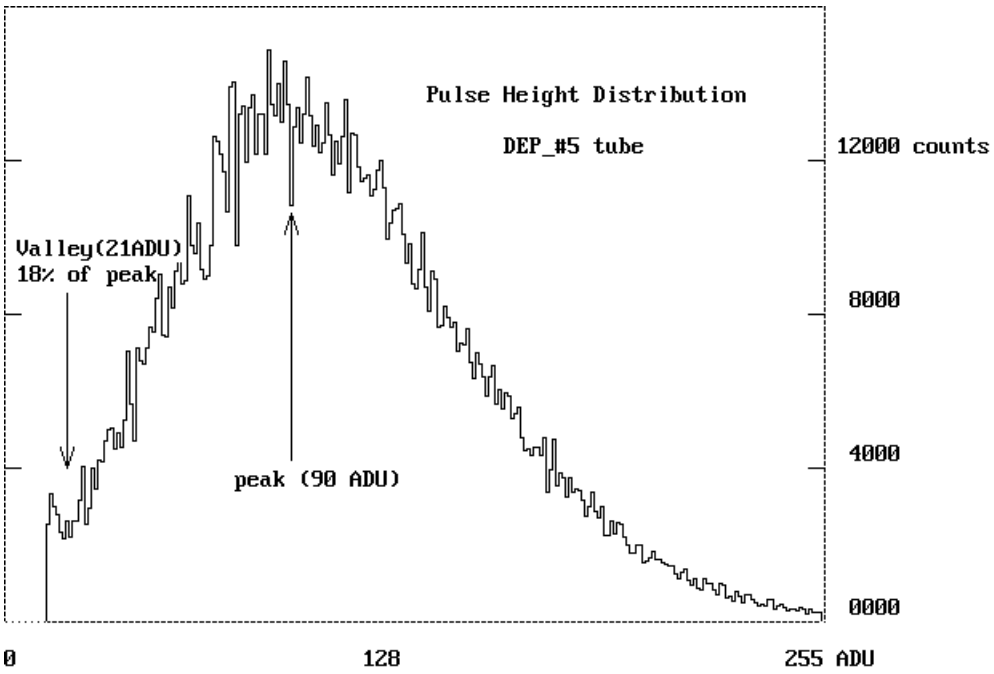

6_4 16H 49M 50S 1998/07/21/
[illegible]96 PHD 746,867cnt/10000FR 400-2370-5400 DEP-5

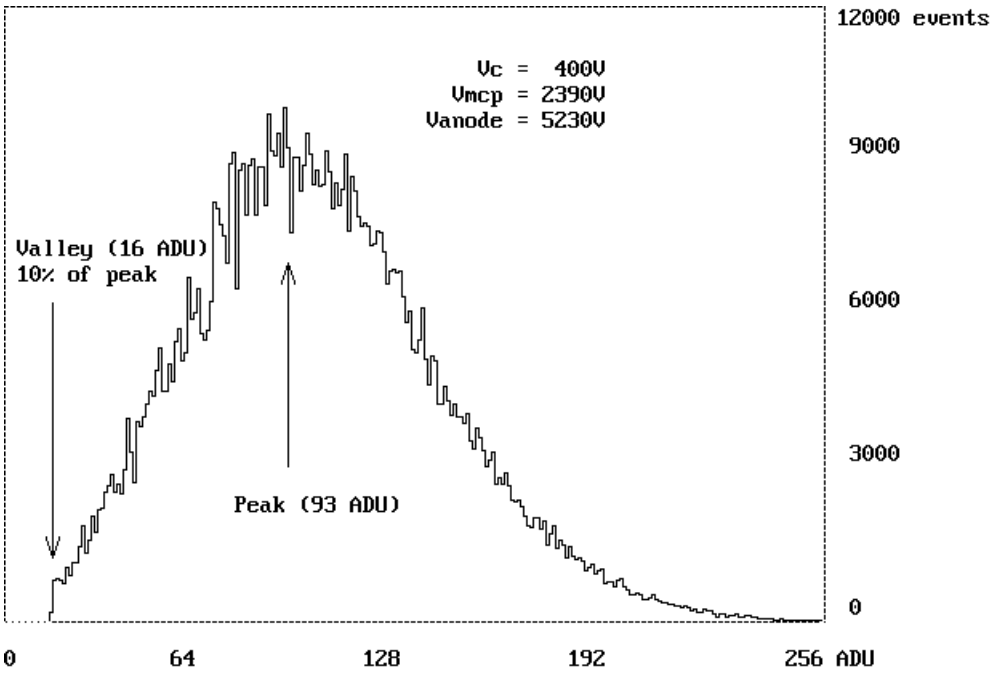

6_5
Pulse Height Distribution of DEP #6 tube

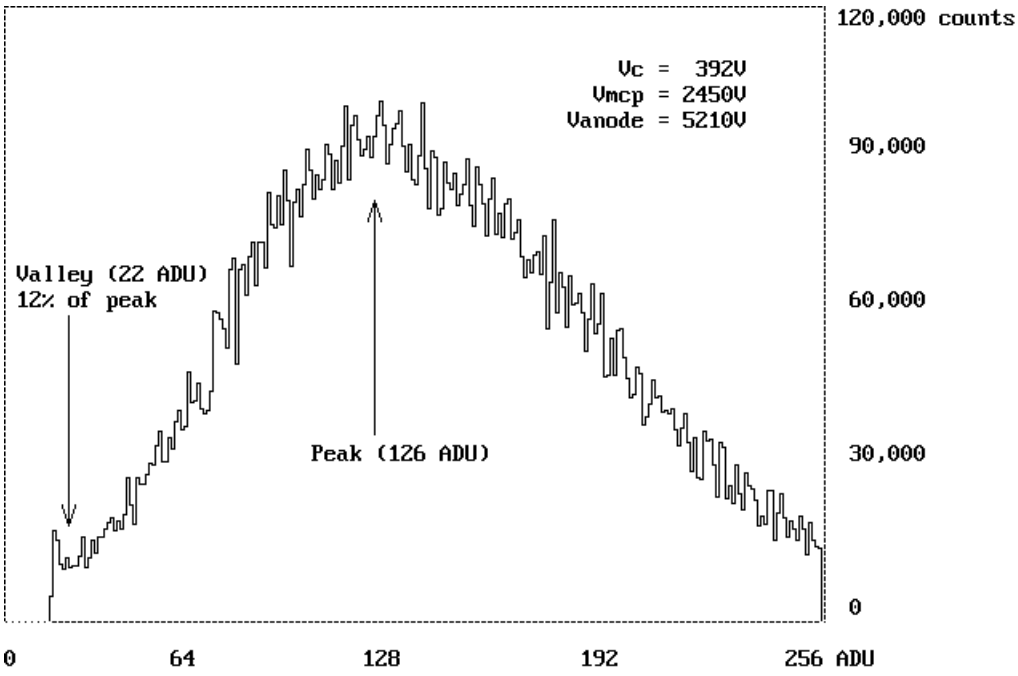

6_6
Pulse Height Distribution of DEP #7 tube

Figures 6_7, 6_8 and 6_9 show the pulse height distributions from different places along x-direction with the DEP_#1, #4 and #6 intensifiers. The gain variation across the 6 intensifiers is quite large. The science window region of the detector was divided into 8x8 sectors, and the gain at each sector was measured. The results are

tabulated in Table 6_2 for 5 intensifiers. The table does not contain the data on DEP_#4, because MSSL's data acquisition system was broken during the delivery of the 2nd FM detector. The #6 and #7 intensifiers from the 3rd batch and the #5 intensifier from the second batch show monotonic gain increase from left to right. The DEP_#4 and #6 intensifiers show the smallest gain variation. Since the gain variation of the DEP_#7 intensifier was large, a higher voltage had to be applied to Vmcp, in order to suppress the gain variation. As the consequence, the gain in the right hand side became too high and caused many SIBs. These SIBs are seen as a noise component at the low energy end in figure 6_6.

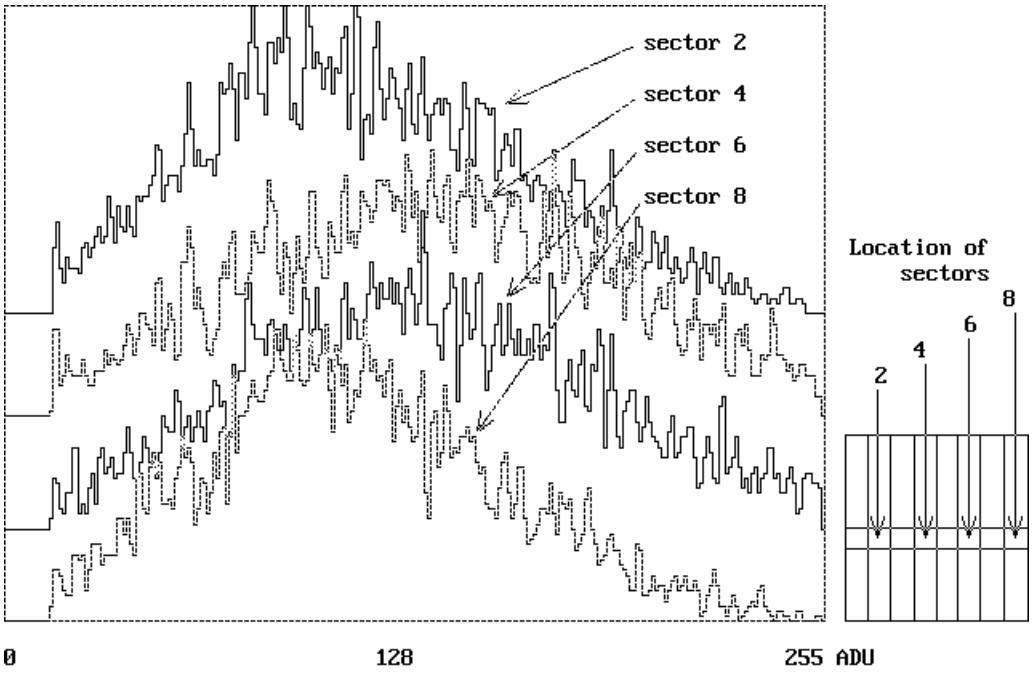

6_7
Variation of pulse height distribution DEP_#1 tube

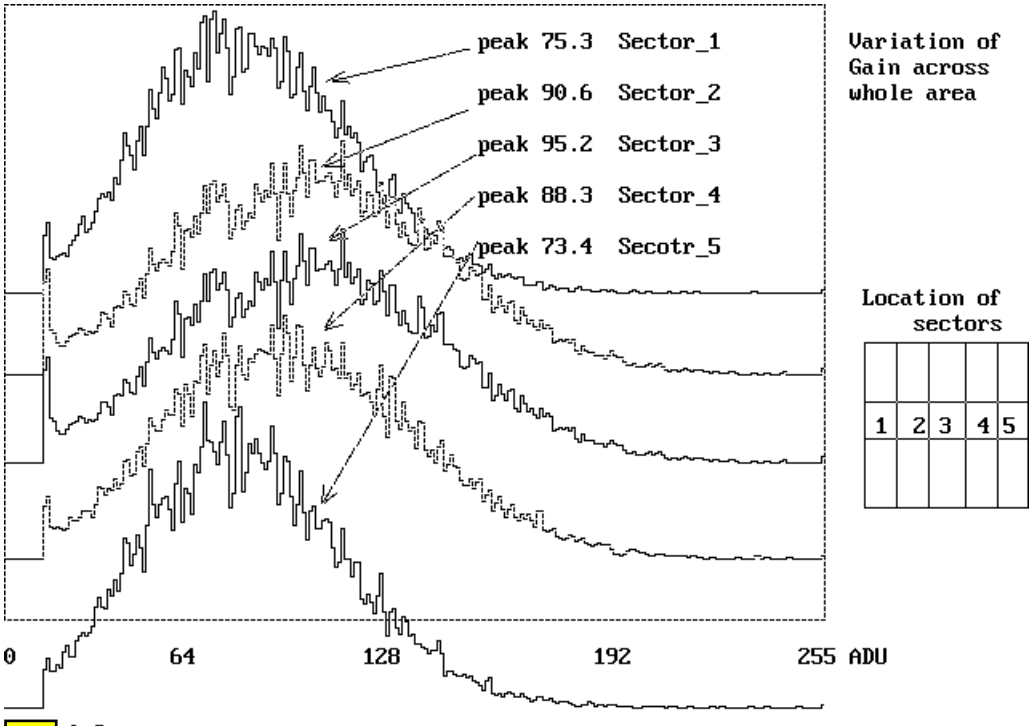

6_8
Pulse Height Distribution of DEP FM_#4 tube

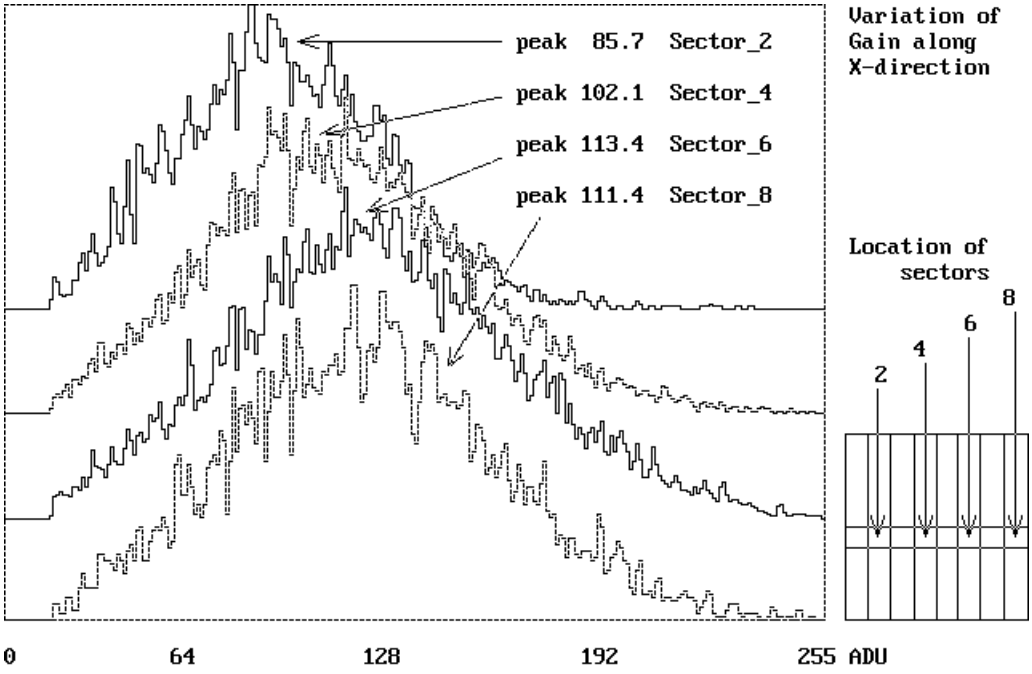

6_9
Pulse Height Distribution of DEP_#6 tube

Table 6_1. Pulse height distribution from 256x256 area

	DEP_#1	DEP_#2	DEP_#4	DEP_#5	DEP_#6	DEP_#7
Vmcp	2200V	2200V	2310V	2360V	2400V	2450V
dG/G	129%	134%	110%	121%	97%	111%
Peak/Valley pos	5.3	6.0	4.3	4.3	5.8	5.7
Valley depth (relative to peak)	18%	14%	19%	18%	10%	12%
Gain Variation	60%p-p	50%p-p	30%p-p ?	60%p-p	40%p-p	60%p-p

Table 6_2. Individual gains at 8x8 sectors

DEP_#1 tube 14 March 1998 <=== PHD006.DAT

.81	.95	1.03	1.08	1.11	1.07	.99	.86
.84	1.02	1.16	1.22	1.21	1.20	1.08	.98
.87	1.10	1.22	1.33	1.29	1.30	1.19	1.02
.86	1.07	1.22	1.32	1.34	1.28	1.20	1.00
.83	1.03	1.20	1.28	1.25	1.23	1.17	1.01
.77	.95	1.09	1.14	1.20	1.13	1.03	.96
.72	.83	.95	1.02	1.00	1.00	.92	.85
.63	.78	.84	.88	.87	.87	.80	.72

DEP_#2 tube 12 March 1998 <=== PHD003.DAT

.85	.90	.95	.96	1.10	.96	.99	.79

.93 1.07 1.00 1.11 1.11 1.10 .99 .90

1.00 1.01 1.05 1.14 1.21 1.16 1.09 .95

.99 1.03 1.04 1.59 1.20 1.25 1.18 1.03

.80 .97 1.11 1.08 1.21 1.02 1.13 .98

.75 .89 1.01 1.13 1.12 1.12 1.10 .92

.72 .82 1.14 1.07 1.03 1.06 .93 .97

.65 .78 .77 .88 .88 .94 .88 .84

DEP_#5 tube 21 July 1998 <=== DEP196.DAT

.59 .70 .77 .82 .84 .82 .78 .74

.71 .82 .90 .95 .99 .97 .94 .84

.81 .92 1.03 1.11 1.13 1.10 1.07 .99

.89 1.01 1.14 1.24 1.28 1.25 1.16 1.08

.93 1.07 1.21 1.32 1.37 1.33 1.22 1.13

.93 1.07 1.20 1.33 1.37 1.35 1.27 1.17

.89 1.02 1.14 1.26 1.29 1.30 1.22 1.14

.84 .98 1.07 1.13 1.19 1.20 1.16 1.01

DEP_#6 tube 1 July 1998 <=== DEP124.DAT

.79 .89 .96 1.03 1.09 1.11 1.08 1.02

.85 .92 .99 1.07 1.12 1.13 1.11 1.09

.87 .94 1.01 1.08 1.15 1.18 1.18 1.15

.87 .92 1.00 1.10 1.17 1.22 1.21 1.20

.85 .91 1.01 1.10 1.14 1.19 1.19 1.23

.80 .86 .93 1.02 1.09 1.14 1.15 1.17

.76 .80 .87 .94 1.01 1.04 1.10 1.11

.74 .78 .80 .85 .90 .98 1.04 1.03

DEP_#7 tube 30 June 1998 <=== DEP118.DAT

.69 .81 .89 .98 1.06 1.13 1.16 1.17

.75 .83 .94 1.05 1.16 1.23 1.25 1.24

.77 .85 .97 1.12 1.24 1.30 1.32 1.29

.80 .89 1.05 1.21 1.31 1.34 1.33 1.26

.81 .91 1.05 1.20 1.27 1.30 1.26 1.21

.80 .87 .97 1.12 1.16 1.20 1.16 1.09

.79 .82 .87 .98 1.01 1.01 1.00 .94

.77 .79 .82 .87 .88 .88 .88 .85

Ref-6 Files used for this section

/depfm1/zphd006.dat

/depfm2/zphd208.dat

/depfm4/zphd088.dat (<===PHD004.DAT, JLAF-format)

/depfm5/zdep196.dat

/depfm6/zdep124.dat

/depfm7/zdep118.dat

7. Event profile and SIBs

The XMM-OM intensifier output interfaces to a tapered fibre with image reduction of 3.37. This optical configuration contributes to loss of throughput efficiency. Therefore it is difficult to characterize the

detailed profile of an individual event. To capture a faint event image with sufficient S/N, a low noise slow scan CCD camera (manufacture: Santa Barbara Instrument Group, hereafter SBIG CCD camera) was used. It was

coupled to the output end of the tapered fibre via high throughput Nikon camera lenses (85mm/F2.0 + 50mm/F1.4). With these magnifying optics and a small CCD pixel size (9um), a plate scale of 5.5um/pixel was achieved. This corresponds to 18.5um/pixel on the phosphor screen of the intensifier. DEP_#1, DEP_#4 and DEP_#5 were investigated using this setup.

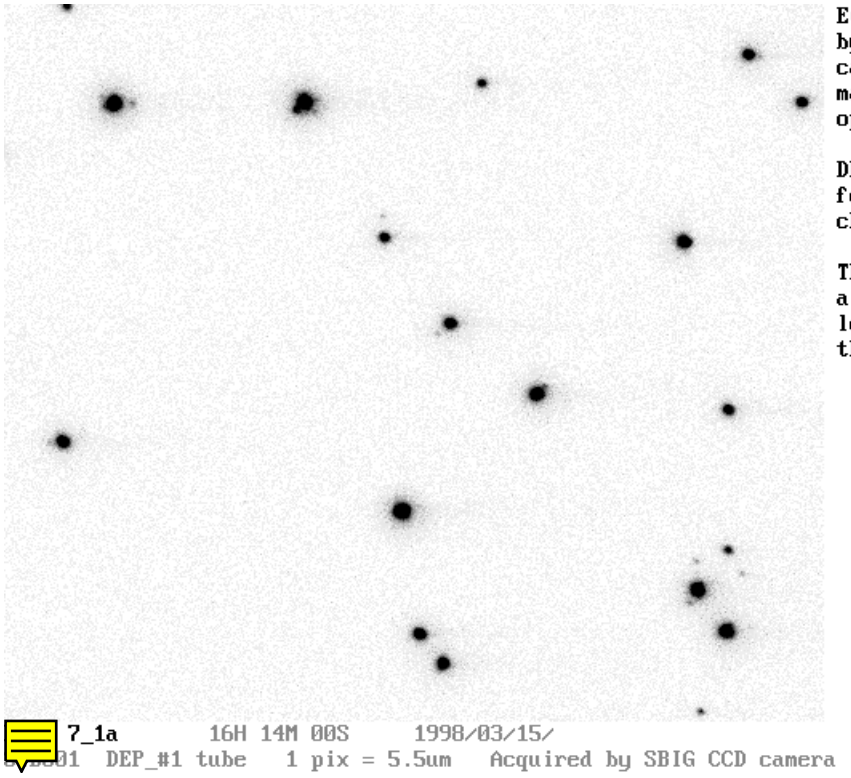

Events captured by SBIG CCD camera with magnification optics.

DEP_#1 tube for FM-primary channel

This tube shows a little higher level of SIB than FM-2ndary

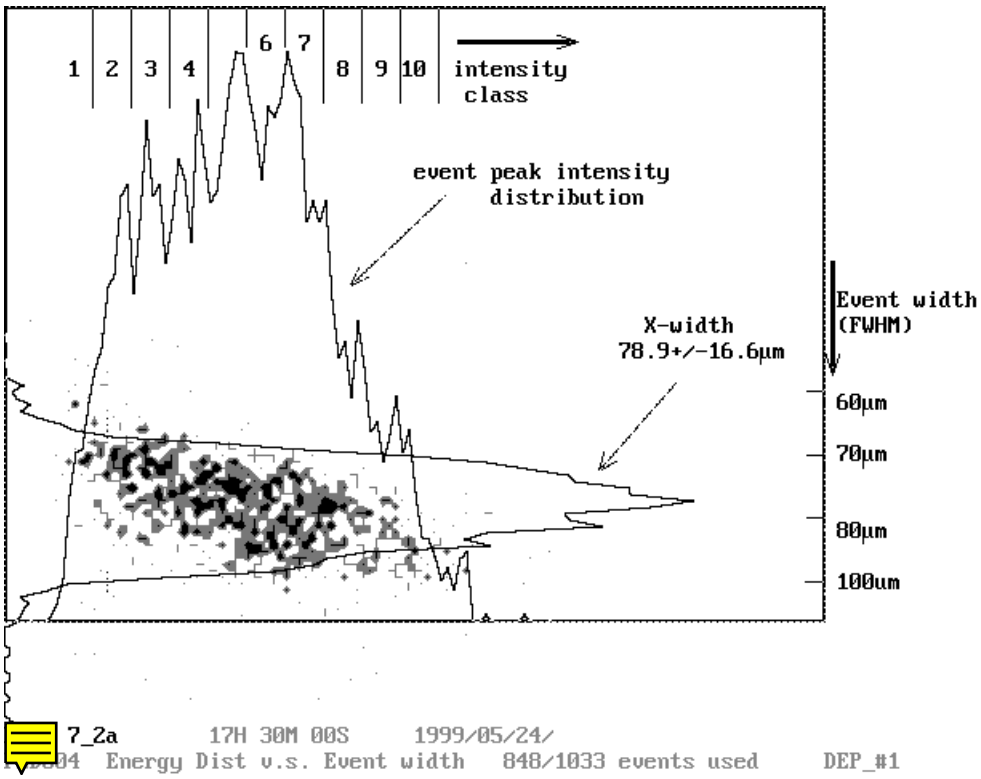

Figure. 7_1a is a snap frame of photo-events at the phosphor screen for the DEP_#1 intensifier. There are satellite events (SIB) around some of the main events. These SIBs broaden the effective event width, hence causing an increase in coincidence. The SIBs also cause a centroiding error, hence degrading the resolution. 64 CCD snap frames were acquired and 848 events were analysed for event width. Fig. 7_2a shows the correlation between the event width and event intensity. The brighter events have broader widths. Average event widths were 79um along X-direction and 74um along Y-direction. These are larger than the ideal but still inside the specification.

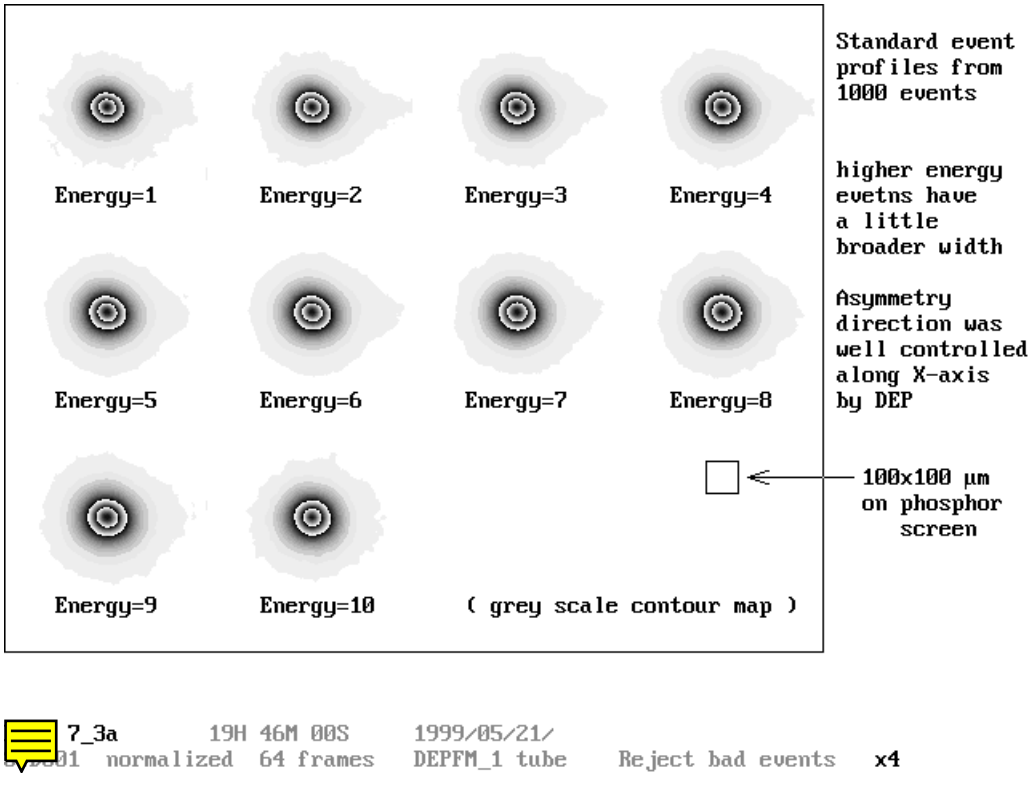

Standard event profiles were made for the DEP_#1 intensifier from the 848 events in Fig. 7_3a. Since event profile depends on event intensity, the events were classified into 10 intensity levels. Events were added on top each other according to their intensity levels. The event shape is nearly round, but major axes of the profiles (clearer in the lower energy events) are aligned to X-axis. This proves that DEP placed MCP2 in the right orientation.

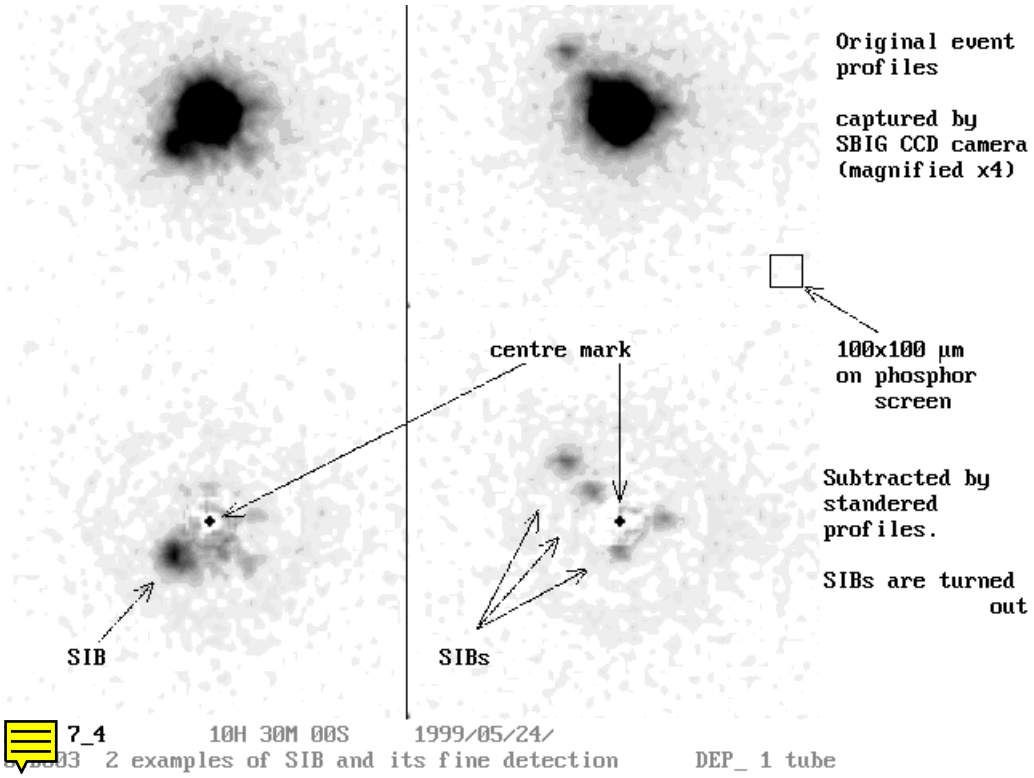

Some of the SIBs are isolated from a main event, but most are semi-detached or hidden inside a main event. Top left in Fig. 7_4 is an example of a semi-detached SIB, and in the top right of Fig. 7_4 is an example of hidden SIBs, which have made the event shape highly distorted. Since it is difficult to measure the energy of the SIBs in the original image even for the semi-detached one, the main event was removed using the standard event profile in corresponding intensity level (bottom of Fig. 7_4). After the removal of the main events, the semi- detached SIB

and the 3 hidden SIBs could be quantified accurately.

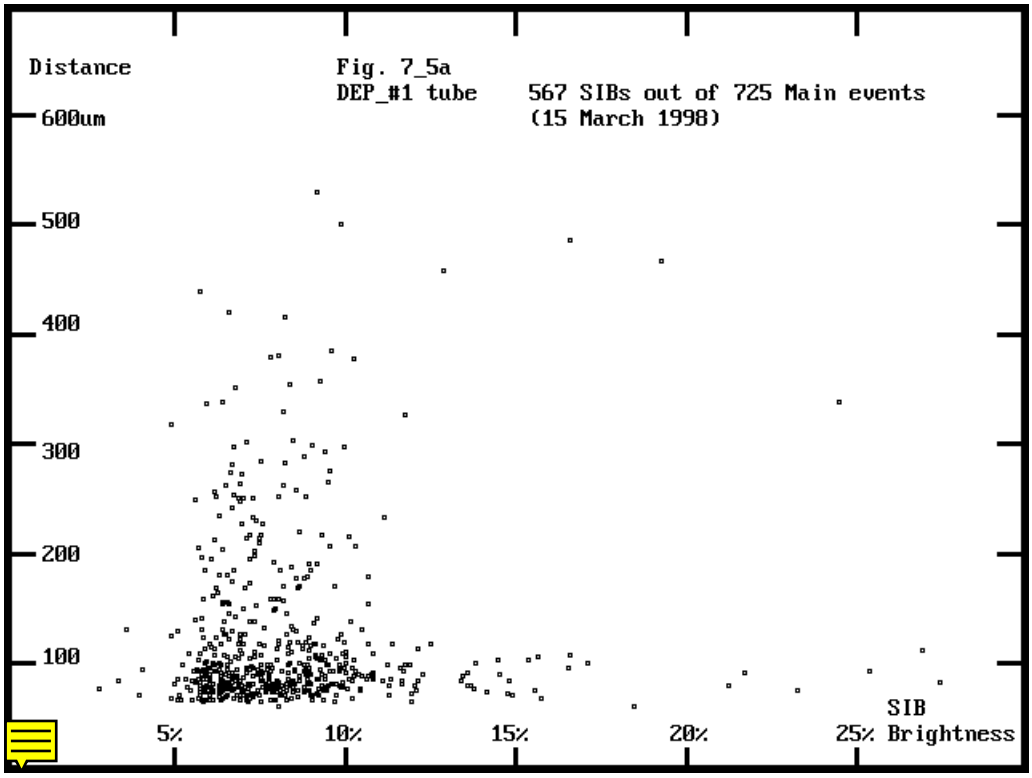
Distance
Fig. 7_5a
DEP_#1 tube 567 SIBs out of 725 Main events
(15 March 1998)
600um
500
400
300
200
100
5%
10%
15%
20%
25%
SIB
Brightness

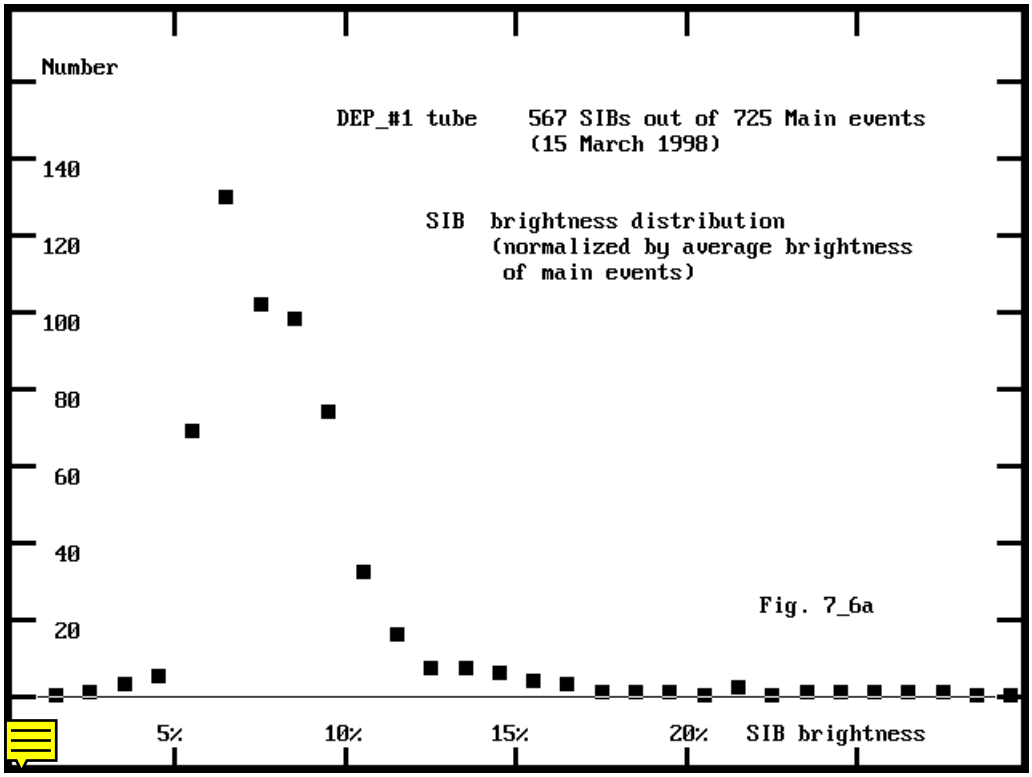
Number
DEP_#1 tube 567 SIBs out of 725 Main events
(15 March 1998)
SIB brightness distribution
(normalized by average brightness
of main events)
140
120
100
80
60
40
20
Fig. 7_6a
5%
10%
15%
20%
SIB brightness

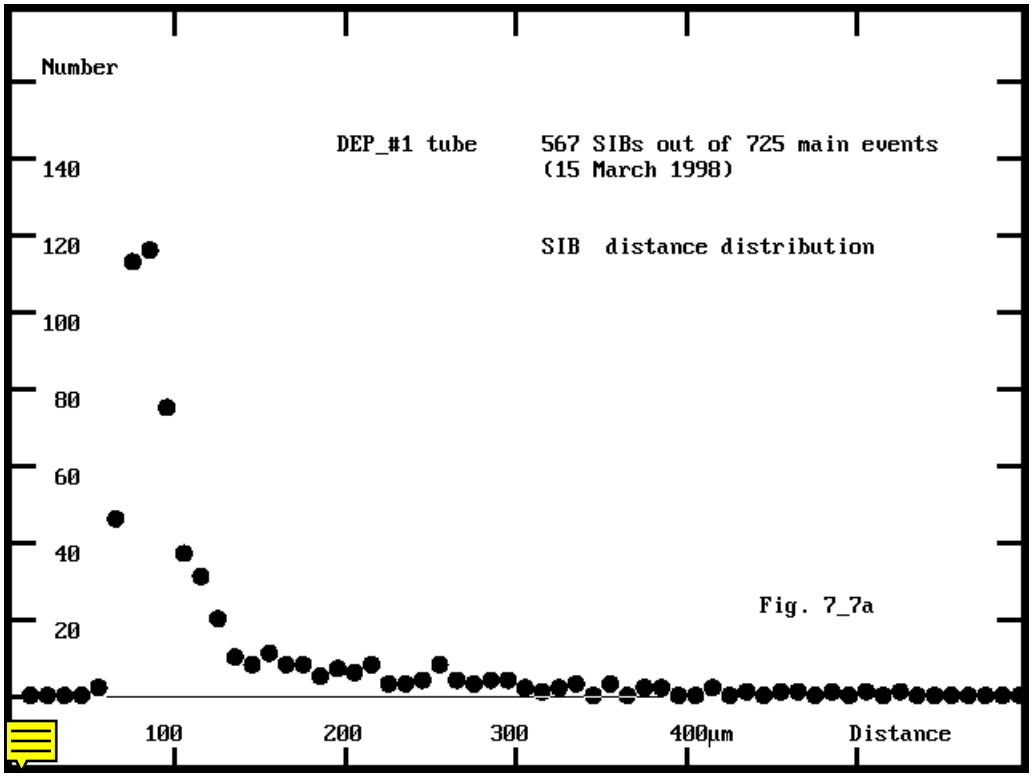

725 main events, which have no neighbouring events within 32 CCD pixels, were used for SIB analysis and 567 SIBs were detected. Fig.7_5a shows the correlation between SIB energy and distance from a main event. Most of

events are located within 100um. It should be noted that a significant number of SIBs whose energies were less than 7% of the main event, were not picked up because of limited S/N. Fig.7_6a shows the energy distribution of the SIBs. There are a significant number of SIBs, but most SIBs have low energy. Only 10% of main events have high energy SIBs (i.e. >10% of the main event energy). There are very few SIBs whose energy is larger than 15% of the main event. Fig.7_7a shows the distance distribution of SIBs. Most of them are semi-detached or inside the main event.

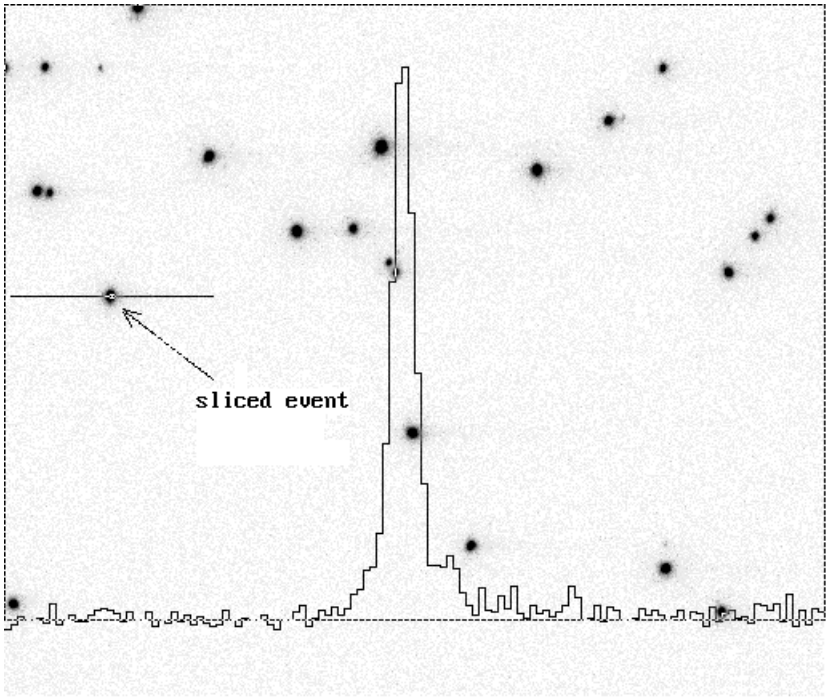

DEP #4 tube
shows SIB-free
event shapes

453-2300-5060
volts

7_1b
#4 tube x3 magnified CCD snap frame (5.29um = 1 pixel)

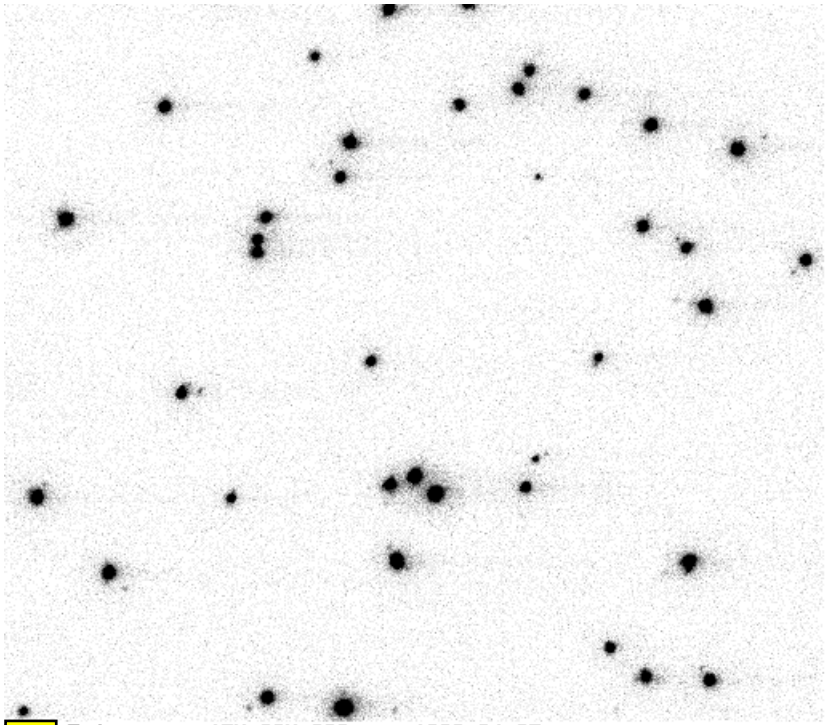

7_1c 15H 38M 00S 1998/04/27/
28 DEP_#5 tube 450-2350-5170 1 pix = 5.5um by SBIG CCD camera

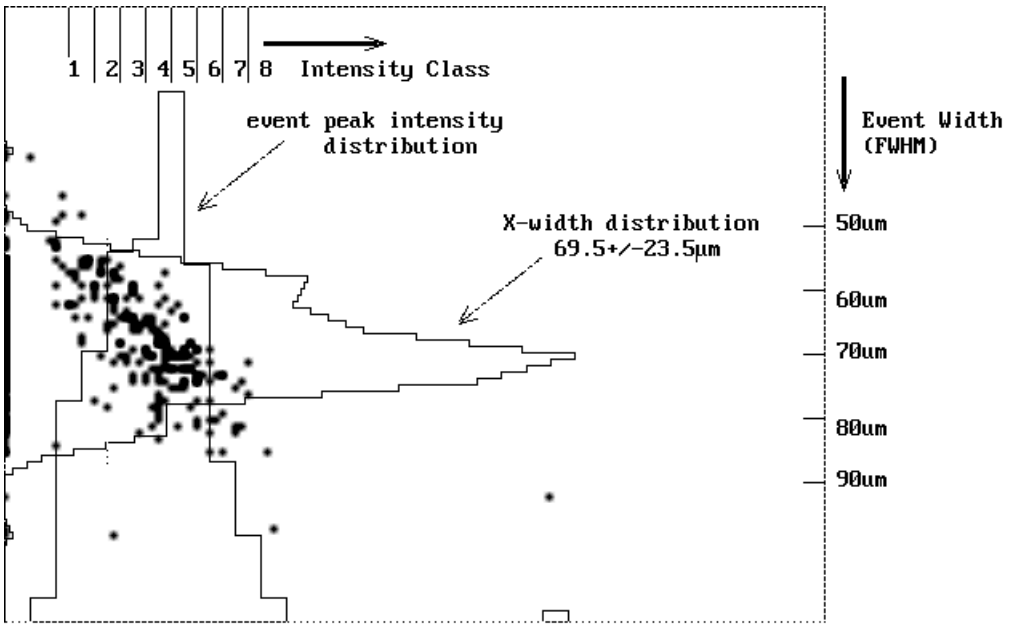

7_2b 12H 50M 00S 1999/06/03/
[illegible]07 Energy Dist v.s. width 158/199 events 453-2300-5060 DEP_#4

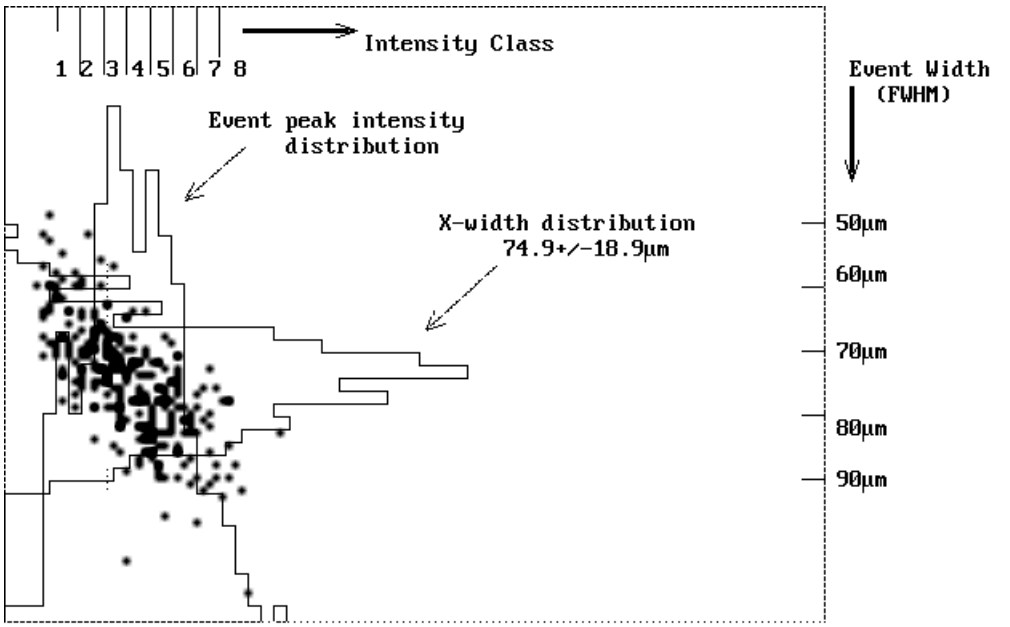

7_2c 11H 10M 00S 1999/06/04/
[illegible]08 Energy Dist v.s. width 203/282 events 450-2350-5170 DEP_#5

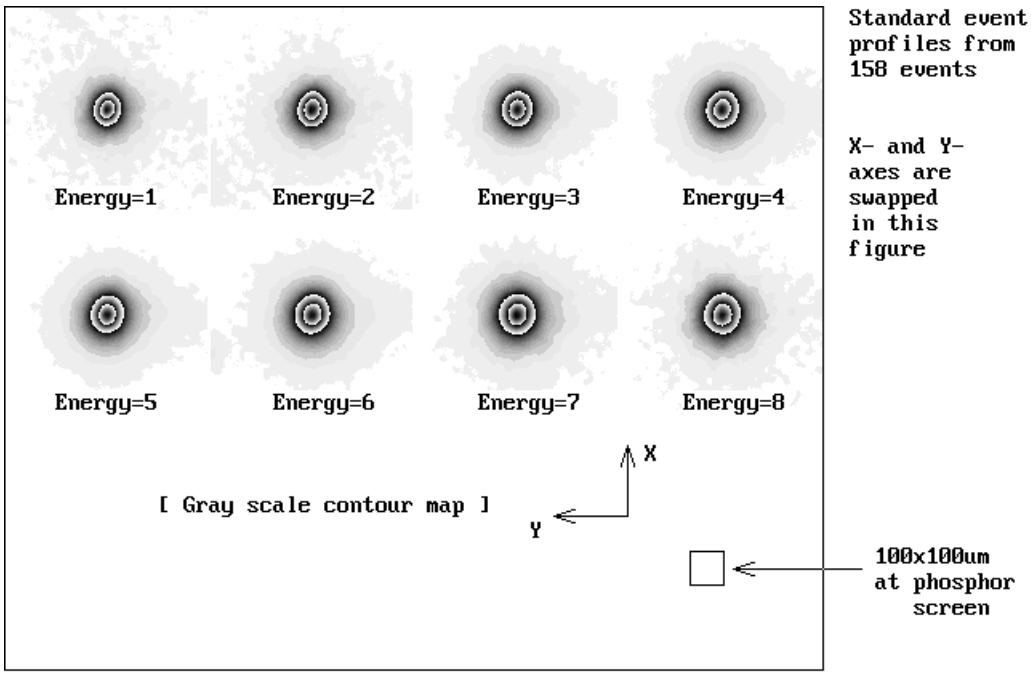

7_3b 12H 50M 00S 1999/06/03/
[illegible]07 Normalized 10FRs 158/199 453-2300-5060 DEP_#4 (70,1000,400)

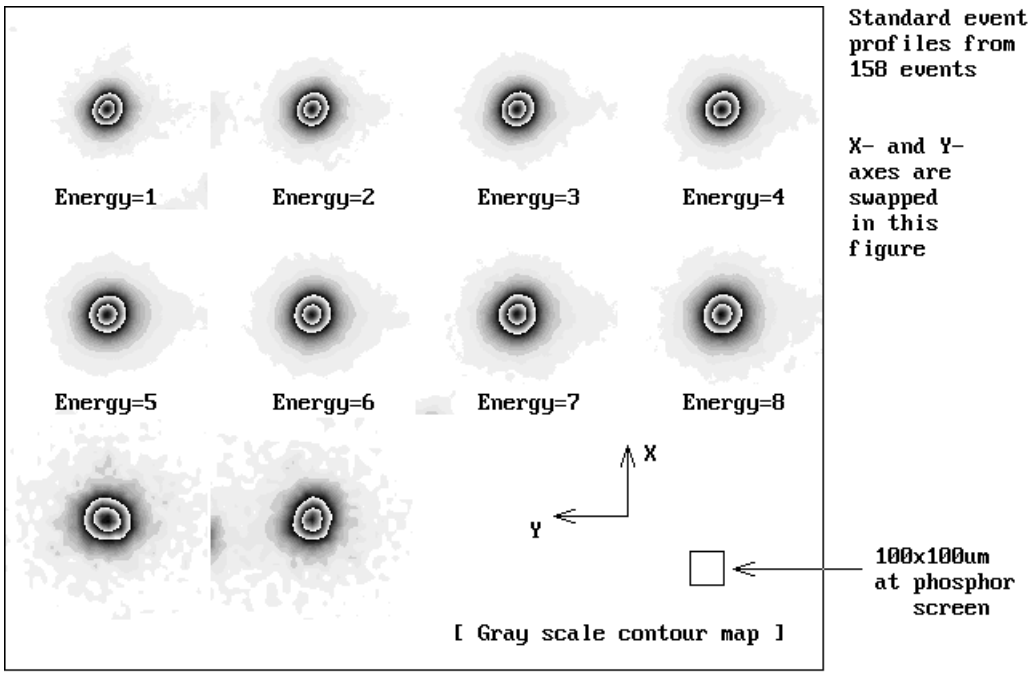

7_3c 11H 10M 00S 1999/06/04/
[illegible]08 Normalized 10FRs 203/282 450-2350-5170 DEP_#5 (60, 840,360)

Figures 7_1b and 7_1c are snap frames of photo-events at the phosphor screen for DEP_#4 and DEP_#5 intensifiers. DEP_#4 intensifier has significantly fewer SIBs than DEP_#1. Figures 7_2b and 7_2c show the

correlation between event width and event intensity. Average event widths were 81um along the X-direction and 70um along the Y-direction for the DEP_#4 intensifier, and 77um along the X-direction, 75um along the Y-direction for DEP_#5 intensifier. These are larger than the ideal but still inside the

specification. Figures 7_3b and 7_3c show standard profiles for DEP_#4 and DEP_#5 intensifiers. The major axes for both intensifiers were misaligned by 12 degrees for DEP_#4 and 20 degrees for DEP_#5.

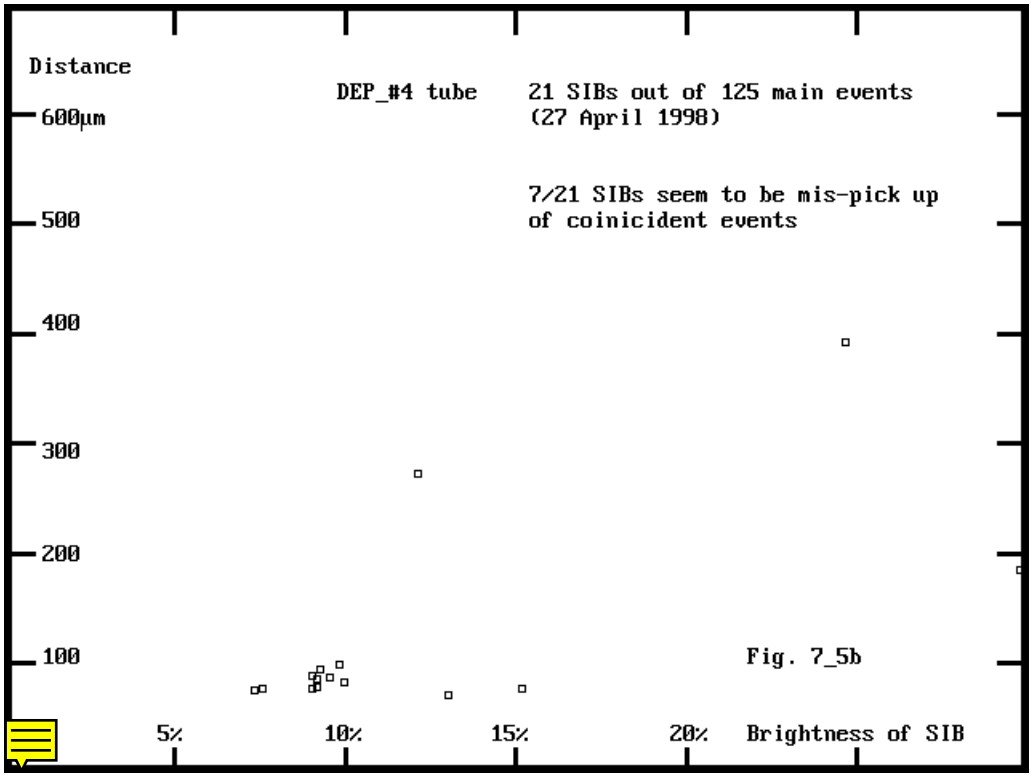

Fig. 7_5b

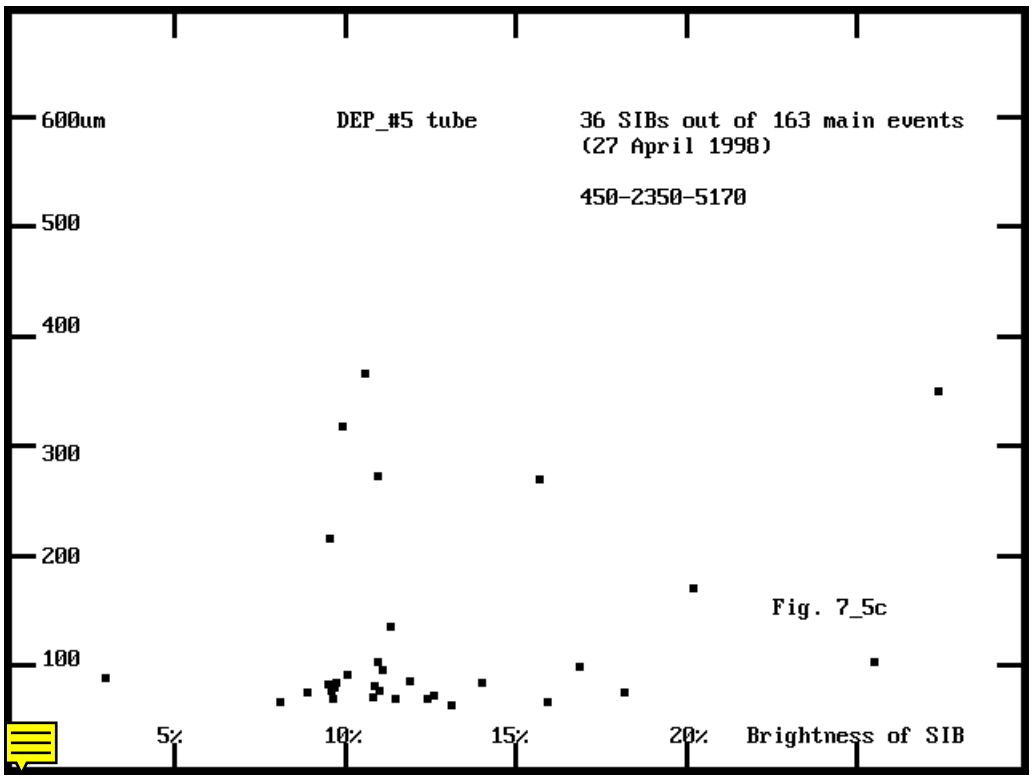

Fig. 7_5c

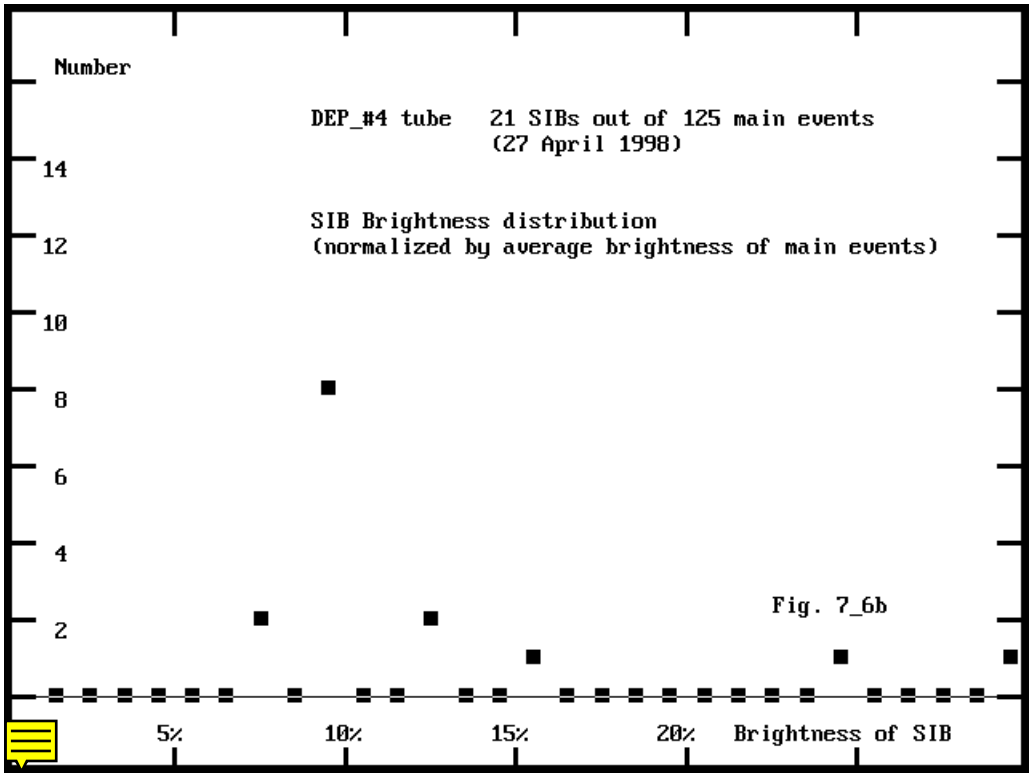

Fig. 7_6b

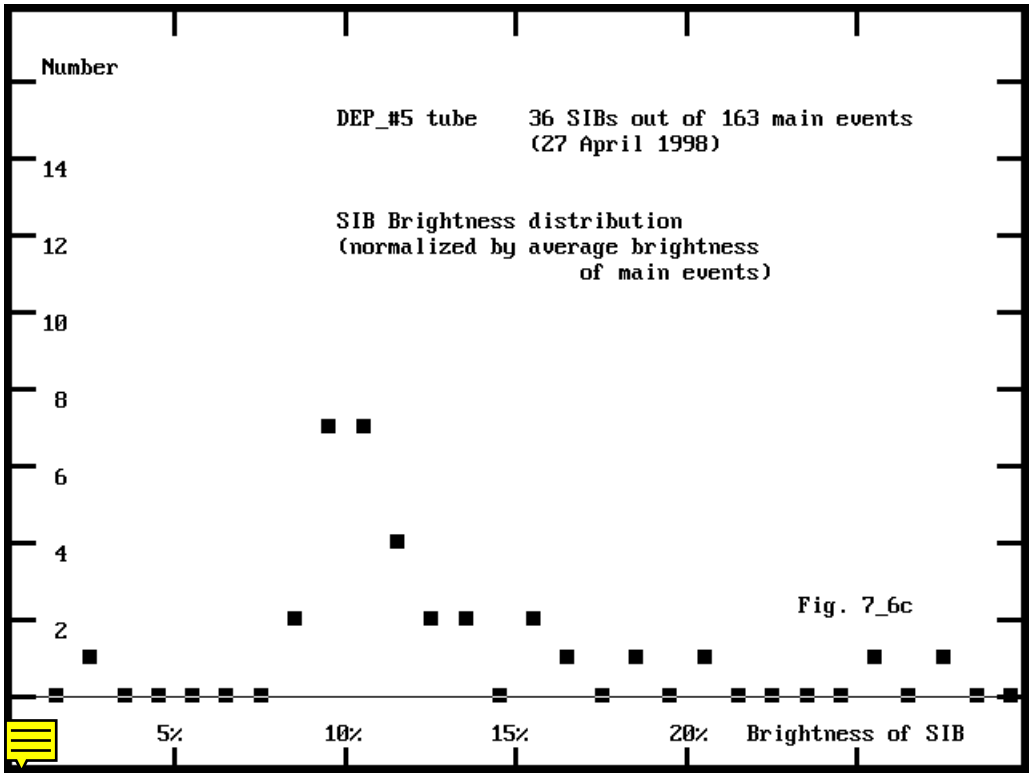

Fig. 7_6c

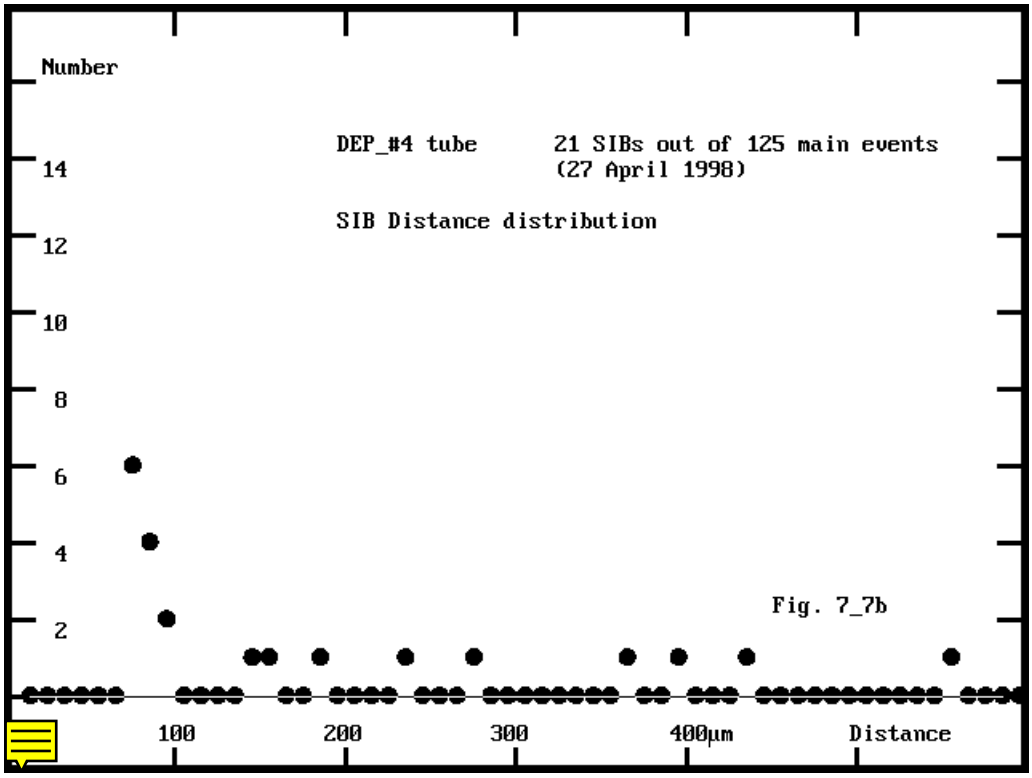

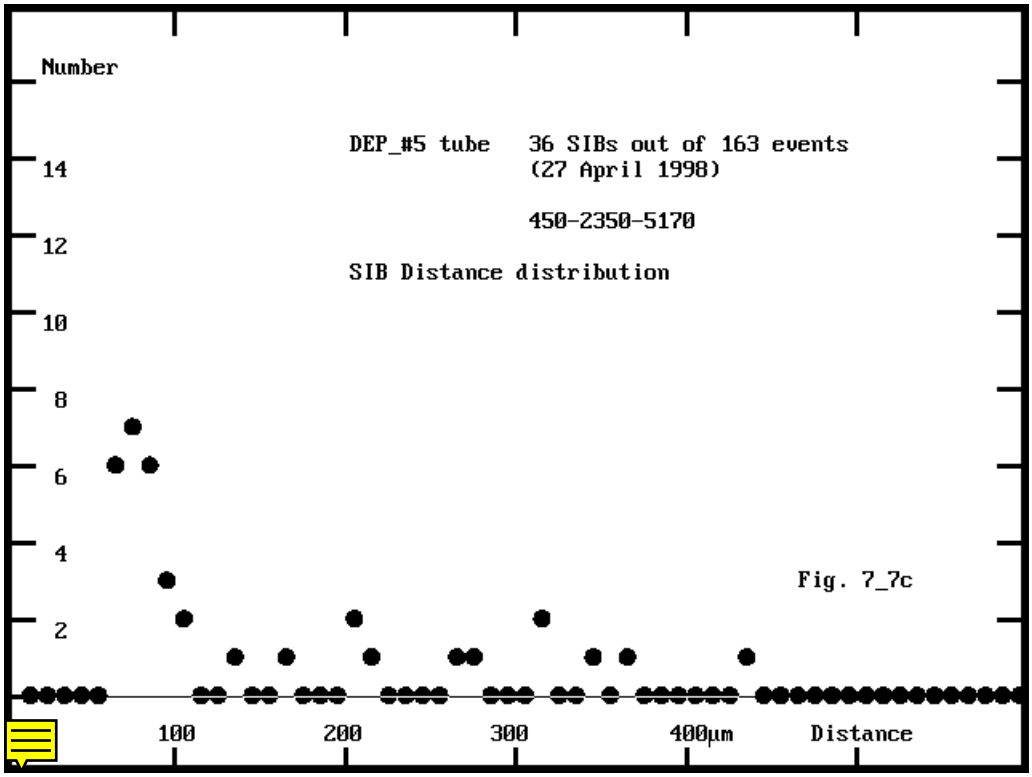

125 isolated main events were used for the analysis of SIBs and 14 SIBs were detected for DEP_#4. 36 SIBs out of 163 main events were detected for DEP_#5. Figures 7_5b and 7_5c show the correlation between the SIB

energy and distance for DEP_#4 and DEP_#5 intensifiers. Figures 7_6b and 7_6c show the energy distribution of the SIBs. Figures 7_7b and 7_7c show the distance distribution of the SIBs. Very few SIBs were detected,

particularly for DEP_#4 intensifier. The event profiles were investigated only with the MIC-CCD camera

for

DEP_#6 and DEP_#7 intensifiers. Because of its undersampling, the event size cannot be quantified. An upper limit to the event width, however, can be estimated; if it were too large, it would have been measurable.

SIBs of the #6 intensifier were not detected with the MIC-CCD camera. A noticeable number of SIBs were detected in the right hand side of the #7 intensifier even by MIC-CCD camera. These SIBs are the side effect of

too high a gain in the region as mentioned in section 3. Unfortunately, EEV CCDs have already been bonded to the DEP_#6 and DEP_#7 intensifiers. Therefore, these two intensifiers can no longer be investigated by the

SBIG CCD camera.

Table 7_1. Event profile

	DEP_#1	DEP_#4	DEP_#5
event X-width	79um	81um	77um
event Y-width	74um	70um	75um
orientation of major axis	0 deg	-12 deg	-20 deg
SIBs (> 7.5% energy of main events)	49%	11%	21%

Ref-7 Files used for this section

/depfm1/sbig/zdep001.dat - zdep064.dat

zdrk001.dat

zstd001.dat

zphd004.dat

/depfm4/sbig/zdep001.dat - zdep010.dat

zstd007.dat

zphd007.dat

/depfm5/sbig/zdep021.dat - zdep030.dat

zstd008.dat

zphd008.dat

8. Ruggedness

8-1. Current consumption

Current leakages at the photocathode gap and at the anode gap are indications of tightness and reliability of the mechanics. The current between MCP_in and MCP_out is dominated by the flying current through the

MCPs, but is useful for checking for any damage to the MCPs. It is, of course, important to know, as the main power consumption of an intensifier occurs here and can cause trouble with the HV unit if the

consumption is too high. DEP produced 7 image intensifiers for XMM-OM. Two out of the seven were delivered to ESA as the FM detector, leaving only the remaining 5 intensifiers to be measured. The currents of the

two FM intensifiers were estimated from other intensifiers. The anode gap and photocathode gap showed extremely high impedance as expected. The results are tabulated in table 8_1. The expected currents at nominal operating voltages are in table 8_2. These exceptionally low currents were measured using the amplifier made for the R.Q.E measurement, which can provide 44V by batteries to two arbitrary terminals (XMM-OM/MSSL/TC/0053). The anode current of DEP#2 intensifier is larger than those of the other intensifiers. For this reason, this intensifier was delivered to MSSL as a set-up device.

A Keithley 485 Autoranging Picoammeter was inserted between the MCP_in terminal and ground to measure the MCP current. The photocathode gap voltage was closed to zero during the measurement.

The impedance of the

MCPs changed with the MCPs voltage (see table 8_3), but the change was less than 5% between 1000 - 1800V. The current at the nominal operation voltage, 2400V, was estimated from the impedance at 1800V. The nominal

current varies from tube to tube (i.e. 4.5-6.4uA), but all were far below the maximum current of the FM H.V. unit, 30uA. These results imply that the two FM intensifiers can be driven by the FM-H.V. unit very easily.

The DEP#6 intensifier, which has shown excellent resolution at UV wavelengths and has been kept as Spare_#1, showed very little anode current and relatively low photocathode current. These indicate the solid mechanics of the intensifier.

The relationship between the impedance and the edge emission is not clear, because the DEP_#7 intensifier has larger leak currents than DEP_#6 at both of photocathode gap and anode gap, but has the smallest edge emission.

8-2. Edge emission

Strong bright circles were seen in the dark images with DEP_#4 and DEP_#5 intensifiers from the 2nd batch (Figures 4_2a and 4_3a). This could be due to arcing at the anode gap, which emits UV light and activates the

edge of MCP1. If so, this is a dangerous sign in these intensifiers. Since then, the edge emission has been carefully re-assessed for all the intensifiers. A weak emission was found in DEP_#1 intensifier at the right hand side edge. There is noticeable emission at the left hand side edge of DEP_#6 extending around 120 degrees. DEP_#7 intensifier has no (or negligible) edge emission but shows switched-on channels (4 c/s cm2) localized at the right hand side. DEP_#8 showed significant edge emission during the acceptance test at DEP. Therefore, all intensifiers

have some symptoms at the edge. Intensities of edge emission at the brightest point are tabulated in table 8_2.

The cause of the edge emission was investigated with the DEP_#4 intensifier to assess the level of danger. The current running through the anode gap was measured with an ammeter by applying 5500V for 35min. The current was too low to be measured by the ammeter. It should not be more than 2.5nA. This level of anode current does not indicate any arcing at the anode gap. The cathode current at 400V was also below that measurable by the ammeter. This current measurement does not indicate arcing at photocathode gap, either. The relationship between the brightness of the edge emission and the photocathode gap voltage, Vc, was investigated by acquiring dark images in photon counting mode for 600sec. Before the experiment, the intensifier was operated in a dark condition overnight to minimize the

effects of fluorescence by window material and trapped electrons at the

photocathode. The room light was off during the dark exposure. Furthermore the detector was held within a light tight box. The results are shown in table 8_4. The D.Q.E. of the intensifier changes slightly with photocathode voltage. The average dark current was used to correct the D.Q.E. effect. The ratio of edge emission to average dark current increases significantly with photocathode voltage.

A very tiny light was added by turning on the room light to investigate the effect of photon feedback from the phosphor screen. The average count (dark+photon) became more than twice; hence the phosphor screen got

more photons, but the edge emission did not change. Therefore, photon feed back is not involved in the edge emission.

Dark images were acquired in photon counting mode with different threshold levels, i.e. changing from 20 ADU(nominal) to 100 ADU. The average dark current reduced by 1/2.5, while the edge emission by 1/12.

This shows that the energy of the edge emission events are lower than ordinary photons (table 8_5). Figures. 8_1 and 8_2 are pulse height distributions for edge emission and for ordinary events with DEP_#4 and DEP_#5 intensifiers. These is direct evidence that the energy of the edge emission is low (1/3 of that of ordinary events).

The four results described above suggest that a small number of UV photons (a few 10s/sec of UV photons), which are related to the current leakage at photocathode gap, hit the edge of MCP1 and generate low energy event.

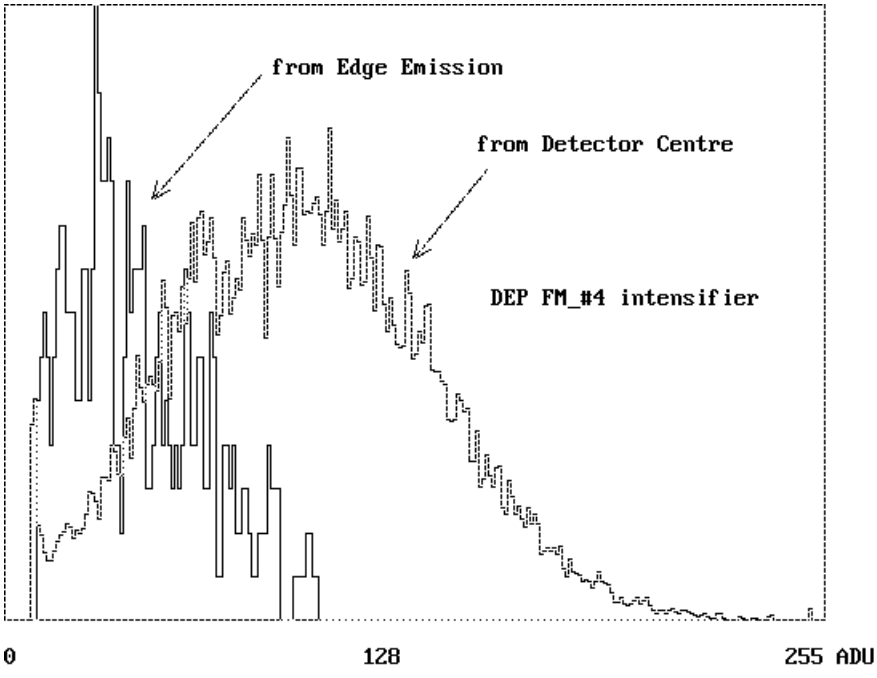

8_1
Pulse Height Distribution from Edege emossion and detector centre

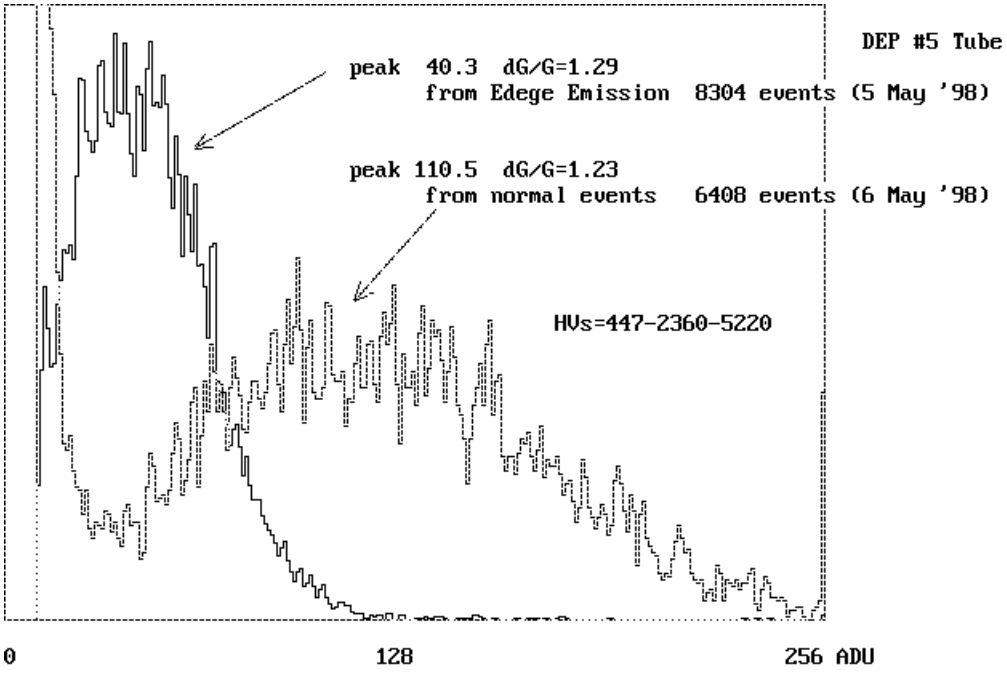

8_2
Pulse height distribution of edge emission compared with normal events.

8-3. Flash

The intensifiers with low dark current (i.e. DEP_#4,#5,#6,#7) and #8 show flashes every 5-10 sec. This might be an indication of weakness of mechanics or short life time of the intensifiers. Only the #1 intensifier did not show noticeable flashes, though the flash might be hidden by the relatively high dark current.

The flashing was investigated quantitatively with the #7 tube. 100,000 CCD snap frames were acquired in the dark conditions with Vc=ON. Most of snap frames contain only 0-2 events, but some of frames received more

than 40 events. The event distribution is tabulated in table 8_6. If a flash is defined as >10 events/frame, then flashes occured with a mean interval of 6 seconds (table 8_7).

Table 8_1. Resistance of tube body (unit: Ohm)

	DEP_#2	DEP_#5	DEP_#6	DEP_#7	DEP_#8
Ph-cath gap (at 44V)	40.8E+12	6.9E+12	15.9E+12	9.9E+12	9.1E+12
across MCPs (at 1800V)	377E+ 6	420E+ 6	405E +6	380E+ 6	531E+ 6
Anode gap (at 44V)	0.063E+13	2.5E+13	34.E+13	6.9E+13	5.1E+13

Table 8_2. Expected current at nominal operating voltages

Nominal voltage	DEP_#1	DEP_#2	DEP_#4	DEP_#5	DEP_#6	DEP_#7	DEP_#8
Vc = 400V	---	9.8pA	0 ?	58pA	25pA	41pA	44pA
Vmcp=2400V	---	6.4uA	5.8uA	5.6uA	5.9uA	6.3uA	4.5uA
Va =6000V	---	9821pA	<2.5nA	239pA	18pA	84pA	117pA
Edge emission	70	---	3400	1240	340	7	significantly seen at DEP

Note) Anode and photocathode currents of DEP_#4 were measured with an ammeter.

Table 8_3. Current vs. voltage applied to MCPs [unit: uA]

Voltage	#2	#5	#6	#7	#8
0V	0.024	0.012	0.013	0.020	0.010
200V	0.502	0.464	0.488	0.505	0.359
400V	1.001	0.918	0.951	1.016	0.732
600V	1.519	1.378	1.441	1.540	1.100
800V	2.044	1.862	1.920	2.052	1.462
1000V	2.551	2.330	2.405	2.588	1.837
1200V	3.096	2.812	2.909	3.113	2.211
1400V	3.640	3.294	3.416	3.653	2.600
1600V	4.200	3.796	3.920	4.192	2.996
1800V	4.779	4.288	4.444	4.743	3.388

11 May 1999

Table 8_4. Edge emission v.s. photocathode voltage

Vc	dark at centre	edge emission	room light	ratio
450	10.8 c/s cm2	3149 c/s cm2	off	292
50	7.2	726	off	101
450	25.0	3050	on	122
50	15.6	684	on	44

Exposure=600sec DEP_#4 tube

Table 8_5. Edge emission v.s. threshold level

Threshold	dark at centre	edge emission	room light	ratio
20ADU	12.14 c/s cm2	4456 c/s cm2	off	367
100ADU	4.85	364	off	75

Exp=600sec Vc=450 Vmcp=2300 Va=5040 DEP_#4 tube

Table 8_6. Statistics of 100,000 CCD frames

Events	0	1	2	3	4	5	6	7	8	9	10	>10	>20	>40
Frame	82932	14544	1747	273	80	57	41	30	34	30	29	164	75	21

Table 8_7. Flash interval

6.0sec	(>10 events/FR)
13.3sec	(>20 events/FR)
47.6sec	(>40 events/FR)

Ref-8 Files used for this section

/depfm1/zdrk009.dat

CDROM/dp414.raw - dp419.raw

/dp421.raw - dp422.raw

/dp423.raw - dp424.raw

/dp410.raw

/dp507.raw

/dp514.raw

/dp605.raw

/dp608.raw

/dp706.raw

/dp707.raw

/depfm4/phd4edg.dat

/depfm5/phd5edg.dat

phddrk.dat

/depfm2/zfsh214.dat - zfsh220.dat

/depfm5/zfsh198.dat

/depfm7/zfsh199.dat - zfsh207.dat

9. Summary and acknowledgement

Characteristics of individual intensifiers are summarized in table 9_1, 9_2 and 9_3 for selected items.

Biggest acknowledgement goes to DEP, who contributed outstanding efforts to producing decent

intensifiers in a very short time period.

Mr. Jon Lapington, MSSL, gave advice on the design of the FM-intensifer. He also used great skill in fixing the intensifier arcing problem in the initial test.

Mr. Graham Willis, MSSL, undertook a significant part of the electrical/mechanical assembly of the intensifiers.

A data acquisition system was borrowed from the Department of Physics and Astronomy, UCL, during the delivery of the FM detectors.

Finally, thanks go to Prof. Keith Mason, PI of XMM-OM, and Prof. Alan Smith, project manager of XMM-OM, for their encouragements and supports.

One of the author (HK) wishes to express personal thanks to Prof. Len Culhane, Dr. Mark Cropper and Mr. Phil Guttridge for their help in many aspects throughout this project.

Table 9_1 Summary of DEP tubes 1st batch

		DEP_#1 (FM-1) F804502	DEP_#2 (loan) F804501
Resolution	@630nm	9.24um	8.44um
	@460nm	17.7um	16.3um
RQE	@300nm	24.35%	25.21%
	@520nm	10.17%	11.01%
Dark (c/s cm2)		80	---
MCP voltage		2200 V	2200 V
dG/G		129%	134%
Peak/Valley position		5.3	6.0

Valley depth	18% of peak	14% of peak
Gain Variation	60%p-p	50%p-p
SIBs (> 7.5% energy of main events)	49%	---
Event size (average)	79um _X 74um _Y	---
Turn-on channel	none	4 Big spots
Blemishes (>50um)	10 black	11 black
edge emission	70c/s/cm2	---
Flash	not noticed	every 5sec

Table 9_2 Summary of DEP tubes 2nd batch

	DEP_#4 (FM-2) F813105	DEP_#5 F813101	
Resolution @630nm	---	---	(Vc=400V)

	@460nm	18.2um	18.1um	(Vc=450V)
RQE	@300nm	25.34	24.45	
	@520nm	11.87	11.31	
Dark (c/s cm2)		13.3	10	
MCP voltage for nominal gain		2310 V	2360 V	
dG/G		110%	121%	
Peak/Valley position		4.3	4.3	
Valley depth		19% of peak	18% of peak	
Gain Variation		30%p-p ?	60%p-p	
SIBs (> 7.5% energy of main events)		11%	21%	
Event size (average)		81um _X 70um _Y	77um _X 75um _Y	
Turn-on channel (Vc=0) (>0.05c/s)		none	1 edge emission covering 120 deg	
Blemishes (>50um)		1 black	2 black 2 white	
Edge emission		3400c/s/cm2	1240c/s/cm2	
Flash period		5sec	7sec (>10 events/FR)	

12sec (>20 events/FR)

33sec (>40 events/FR)

Table 9_3 Summary of DEP tubes 3rd batch

		DEP_#6 (Swift-1)	DEP_#7 (Swift-2)	
		F813104	F813102	
Resolution	@630nm	7.086um		(Vc=400V)
	@460nm	13.5um (LED)	20.2um (LED)	
RQE	@300nm	25.04	23.94	
	@520nm	11.07	10.37	
Dark (c/s cm2)		11	7.4	
MCP voltage for nominal gain		2400 V	2450 V	
dG/G		97%	111%	
Peak/Valley position		5.8	5.7	
Valley depth		10% of peak	12% of peak	
Gain Variation		40%p-p	60%p-p	

SIB	similar to DEP_#4	similar to DEP_#1
Event size	---	---
Turn-on channel (Vc=0) (>0.05c/s)	None	None
Blemishes (>50um)	7 black	5 black
Edge emission	340 c/s/cm2	7 c/s/cm2
Flash period	5 sec	5.4 sec (>10 events/FR) 12.8sec (>20 events/FR) 50.0sec (>40 events/FR)
